Development of a Global Fire Weather Database ~~for 1980-2012~~

Robert D. Field[1,2], Allan C. Spessa[3,4], Nurizana Amir Aziz[5], Andrea Camia[6], Alan Cantin[7], Richard Carr[8], William J. de Groot[7], Andrew J. Dowdy[9], Mike D. Flannigan[10,11], Kasemsan Manomaiphiboon[12], Florian Pappenberger[13,14,15], Veerachai Tanpipat[12], Xianli Wang[10]

1. Department of Applied Physics and Applied Mathematics, Columbia University, New York, NY, USA
2. NASA Goddard Institute for Space Studies, New York, NY, USA
3. Department Environment, Earth & Ecosystems, The Open University, Milton Keynes, UK
4. Department Atmospheric Chemistry, Max Planck Institute for Chemistry, Germany
5. Malaysian Meteorological Department, Petaling Jaya, Malaysia
6. Joint Research Centre, European Commission, Ispra, Italy
7. Natural Resources Canada, Canadian Forest Service, Sault Ste. Marie, ON, Canada
8. Natural Resources Canada, Canadian Forest Service, Edmonton, AB, Canada
9. The Centre for Australian Weather and Climate Research, Australian Bureau of Meteorology, Victoria, Australia
10. Department of Renewable Resources, University of Alberta, Edmonton, AB, Canada
11. Western Partnership on Wildland Fire Science, Edmonton, AB, Canada

12. The Joint Graduate School of Energy and Environment, King Mongkut's University of Technology Thonburi, Bangkok, Thailand

13. European Centre for Medium-Range Weather Forecasts, Reading UK

14. College of Hydrology and Water Resources, *Hohai* University, Nanjing, China

15. School of Geographical Sciences, Bristol University, Bristol, UK

Correspondence to: Robert D. Field (rf2426@columbia.edu)

Abstract

The Canadian Fire Weather Index (FWI) System is the mostly widely used fire danger rating system in the world. We have developed a global database of daily~~,~~ ~~gridded~~ FWI System calculations beginning in 1980 ~~from 1980-2012~~called the Global Fire WEather Database (GFWED) gridded to a spatial resolution of 0.5° latitude by 2/3° longitude. Input weather data were obtained from the NASA Modern Era Retrospective-Analysis for Research (MERRA), and two different estimates of daily precipitation from rain gauges over land. FWI System Drought Code ~~(DC)~~ calculations from the gridded datasets were compared to calculations from individual weather station data for a representative set of 48 stations in North, Central and South America, Europe, Russia, Southeast Asia and Australia. Agreement between gridded calculations and the station-based calculations tended to be most different ~~over the tropics~~at low latitudes for strictly MERRA-based calculations. Strong biases could be seen in either direction: MERRA DC over the Mato Grosso in Brazil reached unrealistically high values exceeding DC=1500 during the dry season

but was too low over Southeast Asia during the dry season. These biases are consistent with those previously-identified in MERRA's precipitation and reinforce the need to consider alternative sources of precipitation data. ~~This dataset~~GFWED can be used for analyzing historical relationships between fire weather and fire activity at continental and global scales, in identifying large-scale atmosphere-ocean controls on fire weather, and calibration of FWI-based fire prediction models.

1. Introduction

Fire danger rating systems are used to identify conditions under which vegetation fires can start and spread. This is done by modeling the moisture content of different classes of fuels in response to changing weather conditions, and potential fire behaviour if a fire were to start. The Canadian Forest Fire Weather Index (FWI) System [Van Wagner, 1987] is the most widely used fire danger rating system in the world [de Groot and Flannigan, 2014]. It has operated in its current form in Canada since 1970, and certain components have been adapted for operational use in New Zealand, Fiji, parts of the United States, Mexico, Argentina, Spain, Portugal, Indonesia, Malaysia, and Finland [Taylor and Alexander, 2006] and regionally across Europe [Camia and Amatulli, 2009]. It has been used for estimating future activity in boreal regions [de Groot et al., 2013] and globally [Flannigan et al., 2013] under different climate change scenarios. Because of its use in such a broad range of fire environments, it is central to the ongoing development of real-time global fire danger rating systems [de Groot et al., 2006].

Use of the FWI System either operationally or for research purposes begins with experimental fires and laboratory experiments when possible, expert consultation, and historical analyses of FWI variability and relationships to past fire activity. Historical analyses are possible only after hourly measurements of surface temperature, humidity, wind speed and precipitation are compiled for as many years as available. Typically, these data are from surface weather station networks, and require significant effort in constructing a gap-free record. FWI System maps are usually calculated from geostatistically-interpolated weather fields from the individual stations [Lee et al., 2002].

Recent work has been done to calculate FWI System values from meteorological reanalyses over Portugal and Spain [Bedia et al., 2012], the whole of Europe [Camia and Amatulli, 2010] the Great Lakes region of the US [Horel et al., in press], Siberia [Chu et al., 2014] and globally for use as a baseline against which fire danger in a changing climate can be assessed [Flannigan et al., 2013]. Reanalysis products have their own biases, but remain a critical research tool because of their overall utility [Rienecker et al., 2011]. For the purposes of historical FWI System calculations, they have the advantages over raw weather station data of providing spatially and temporally continuous records based on estimates of weather input fields using the internal, physical consistency of a numerical weather prediction model and modern data assimilation techniques. We argue that ~~They~~ reanalysis estimates provide the only practical means possible of calculating FWI values consistently at continental scales.

This paper describes our development of a global FWI dataset for the period 1980-2012 gridded to a resolution of 0.5° latitude by 2/3° longitude based on the National Aeronautics and Space Administration (NASA) Modern Era Retrospective-Analysis for Research (MERRA) [Rienecker et al., 2011]. Because precipitation in reanalyses tends to be less well-constrained by observations, we also use two global, gridded precipitation datasets. Our goals were to:

i. Provide easily accessible historical FWI System data for new regions of interest.
ii. Provide a consistent and homogenized product for continental and global-scale FWI analyses.
iii. Provide a product that can be easily updated and expanded over time.

This paper is organized as follows. In Section 2, we describe the FWI System components, their input data requirements and procedures for starting and stopping the calculations in cold regions. In Section 3, we describe the meteorological fields used to construct the gridded database and the weather station data against which we compare the gridded calculations. In Section 4, we compare the gridded Drought Code calculations to those from 48 individual weather stations across a representative set of locations, along with a brief description of global patterns in the Fire Weather Index. In Section 6, we summarize the results and suggest options for future development.

2. Description of the FWI System

The FWI System is composed of three moisture codes and three fire behaviour indices [Van Wagner, 1987]. The moisture codes track the moisture content of litter and forest floor moisture content rather, in general, than live fuel moisture. For all codes, increasing values reflect decreasing moisture content, and 'extreme' thresholds are drawn from the Canadian Wildland Fire Information System (CWFIS, http://cwfis.nrcan.gc.ca), but which will be different in other regions. The Fine Fuel Moisture Code (FFMC) is designed to capture changes in the moisture content of fine fuels and leaf litter on the forest floor where fires can most easily start. The FFMC ranges from 0 to 99, which values greater than 91 classified as extreme. The Duff Moisture Code (DMC) captures the moisture content of loosely compacted forest floor organic matter and relates to the likelihood of lightning ignition. It has no upper limit, but values greater than 60 are considered extreme. The Drought Code (DC) captures the moisture content of deep, compacted organic soils and heavy surface fuels. The DC also has no upper limit, but values greater than 425 are considered extreme. The three moisture codes are calculated on a daily basis using the previous day's moisture codes and the current day's weather. The three fire behavior indices reflect the behavior of a fire if it were to start. The Initial Spread Index (ISI) is driven by wind speed and FFMC and represents the ability of a fire to spread immediately after ignition, with values greater than 15 considered extreme. The Buildup Index (BUI) is driven by the DMC and DC and represents the total fuel available to a fire, with values greater than 90 considered extreme. The Fire Weather Index (FWI) combines the ISI and BUI to provide an overall rating of fireline intensity in a reference fuel type and level terrain, with values greater than 30 considered extreme. Additionally, the Daily Severity Rating (DSR) is scaled from the FWI to provide categorical difficulty of control measures. The fire behavior indices reflect surface weather conditions and do not reflect dryness or stability aloft which can also strongly influence fire behavior [Haines, 1988]. Dowdy et al. [2009] provide an accessible description of the underlying equations. Taylor and Alexander [2006] summarize the history behind the FWI System and how different fire management agencies have adopted different components for specific fire management needs.

FWI System calculations require measurements of 12:00 local time (LT) instantaneous temperature at 2 m, relative humidity at 2 m and sustained wind speed at 10 m, and precipitation totaled over the previous 24 hours [van Wagner, 1987]. Measurements are taken in a clearing but the FWI System was designed such that the indices are representative of the conditions within a forest stand. Because each day's calculation requires the previous day's moisture codes, weather records must be continuous and any missing data must be estimated [Lawson and Armitage, 2008]. Too much missing weather data, particularly precipitation, can lead to errors that accumulate over time.

In cold regions, the calculations begin with the arrival of spring and are stopped with the onset of winter. Ideally, the spring startup moisture code values reflect whether or not winter was dry, however this is defined. We based our start-up approach on that of the Canadian Wildland Fire Information System (CWFIS), described at: http://cwfis.cfs.nrcan.gc.ca/background/dsm/fwi. First, snow conditions are examined for the possibility of startup after a winter with substantial snow cover, defined as having a mean snow depth of 10 cm or greater and snow present for a minimum of 75% of days during the two months prior to startup. This requirement was modified from the CWFIS approach of considering snow days in January and February to allow for seasonality in regions other than Canada. In this case, start-up occurs when the station has been snow free for three-consecutive days, and moisture code values representing wet, saturated conditions (DMC = 6, DC = 15) are used. For locations without significant snow cover, startup occurs when the mean daily temperature is 6°C or greater for three consecutive days. The DMC is set to 2 times the number of days since precipitation and the DC is set to 5 times the number of days since precipitation. The FFMC is set to 85 regardless of whether significant winter snow cover was present because of its short memory, with a timelag of 3 days required to lose 2/3 of the free moisture content in light, fine fuels for a standard drying day in Canada, defined has having noon temperature of 21.1°C and 45% RH. The timelag for DMC fuels is ~~12~~ 14 days (rather than the 12 days stated in Van Wagner [1987] (S. Taylor, pers. comm.), and 51 days for DC, reflecting longer equilibration times. The calculations are stopped with either the arrival of snow or a mean temperature below 6°C for three consecutive days.

This approach was chosen to capture the effect of winters with below-normal precipitation, but to avoid fuel and site-specific parameters described in the approach of Lawson and Armitage [2008], which required too much local expert knowledge for our global scope. We also masked out fire-free regions for which the FWI System calculations are not meaningful. Cold regions were excluded based on the requirement that mean annual temperature be greater than -10 C. Desert regions were excluded based on the requirement that mean annual precipitation be greater than 0.25 mm/day. Cells where these criteria were not met were excluded for all years. Based on the temperature criteria, parts of the Canadian and Russian high Arctic were excluded. Based on the precipitation criteria, the Sahara, Gobi and much of the Arabian Peninsula were excluded.

3. Weather data

In this section we describe the meteorological fields used for the gridded FWI calculations and the individual station from regional agencies and data repositories against which the gridded calculations were compared. All data are available as part of the distribution, as is contact information for individual agency sources.

3.1. Gridded fields

The starting point for our calculations was the NASA Modern Era Retrospective-Analysis for Research [MERRA, Rienecker et al., 2011]. MERRA is NASA's state-of-the-art reanalysis product which uses the GEOS-5 atmospheric general circulation model run at ½° latitude × ⅔° longitude horizontal resolution and with 72 vertical levels. Sea surface temperature and sea ice boundary conditions are prescribed from Reynolds et al. [2002]. Observational constraints from a wide variety of in-situ and remotely sensed sources are used. Pressure, temperature, humidity and wind observations are obtained from surface weather stations, upper air stations, aircraft reports and dropsondes, ship and buoy observations, as well as weather satellites and research instruments such as MODIS and QuikSCAT. Raw radiance data are assimilated directly from microwave and infrared sounders with different observational periods, using embedded forward radiative transfer models to estimate instrument-equivalent fields. Precipitation is constrained most directly from Special Sensor Microwave Imager (SSM/I) radiances and Tropical Rainfall Measuring Mission (TRMM) rain rate estimates when available, but not by surface gauges. Further details are provided by Rienecker et al. [2011] and references therein.

Among FWI input variables, the MERRA precipitation estimates are most strongly influenced by the model physics, which, for convective precipitation especially, must be approximated using subgrid-scale parameterizations. This introduces considerable uncertainty into the MERRA precipitation. We therefore considered FWI System calculations using two other daily, global precipitation datasets that are based on rain-gauge data. Sheffield et al. [2006] have produced global 1°×1° fields of meteorological fields useful for land hydrology models. Their precipitation estimates start with monthly precipitation estimates from the University of East Anglia (UEA) Climatic Research Unit (CRU) monthly global gridded product [Mitchell and Jones, 2005] which are distributed at a daily frequency using National Centers for Environmental Prediction (NCEP) / National Center for Atmospheric Research (NCAR) reanalysis [Kalnay et al., 1996].

The National Oceanic and Atmospheric Administration (NOAA) Climate Prediction Center (CPC) produces estimates of global, daily precipitation fields over land from rain gauge data [Chen et al., 2008] at 0.5°×0.5°. Their optimal interpolation method makes use of the covariance structure of the precipitation field, which, compared to more simple distance-only based interpolation methods, should improve estimates where orography is important. The accuracy of gauge-based estimates ultimately depends on the rain gauge density, which for our purpose was most sparse in northern Canada and Alaska, northern Russia, sub-Saharan Africa and equatorial Southeast Asia. The Sheffield and CPC precipitation fields will ultimately share much of the same raw data and should not be considered truly independent. The important differences in this context are in their approaches to interpolation over sparse regions and estimates at a daily time scale. In total, we produced three global FWI System datasets: MERRA only, MERRA with Sheffield (SHEFF) precipitation, and MERRA with CPC precipitation. Throughout the paper we refer to each FWI version by the name of the precipitation input.

Figure 1 shows the mean May snow depth and fraction of days over which the FWI System is active, based on our startup and shutdown procedures. The maps essentially show the dependence and variability of FWI System startup on snow cover as the fire season is starting in at higher latitudes in the northern hemisphere, in this case estimated from MERRA.

3.2. Station data

We compared the calculations from gridded data to those based on individual station data for a representative set of 48 stations obtained from a variety of sources (Table 1). Whenever possible, data was used that had previously been used by individual agencies for FWI System calculations. As such, the length of record varied by agency, as did the pre-processing procedures, which are described below. We sought pairs of stations in the same region to guard against localized effects and possible errors in single weather station records. Similar to the use of the two precipitation datasets, this is not a strict validation of the gridded FWI calculations per se, since some of the weather station data will have been assimilated into the MERRA analyses or the gridded precipitation fields. The comparison to station-based calculations instead provides a sense for users of the smoothing that occurs for grid-cell scale calculations. Individual station calculations were compared to the ~~average~~ mean over the area defined by the station coordinates buffered by a ½-degree latitude and longitude band. Snow depth was generally not available for the station data and was instead sampled from the MERRA estimates. This also simplified our comparison by eliminating DMC and DC startup values as a potential difference between datasets.

Table 1 lists the stations used and the periods covered. The majority of stations were from World Meteorological Organization (WMO)-level synoptic stations and will therefore adhere somewhat to a common set of data quality standards. For consistency, comparison with the gridded FWI calculation was over the period of available data only for each individual station. Additional quality control and gap filling was applied following local procedures that we now describe.

Data for Canadian stations came from Environment Canada for the years 1979 – 1998, 1999 or 2006. Data were available only for the fire season, which was determined using a temperature threshold as outlined in Wotton and Flannigan [1993].

Data for stations in Thailand had no more than 3% missing data for any of the input parameters. Missing data was interpolated temporally or spatially, and subject to established homogeneity tests for temperature and precipitation [Alexandersson, 1986; Manomaiphiboon et al., 2013]. Wind siting was rated at least 'fair' for all stations, indicating the absence of large barriers to unobstructed wind measurements.

For Australia, four pairs of stations were selected with each of these stations having no more than 0.7% of days with missing data for any of the input parameters. Missing data for wind speed, relative humidity and temperature were replaced by the ~~average~~mean of the previous and subsequent days of available data, and missing data for precipitation were replaced by data from the nearby station (using the station pairs listed in Table 1). The rainfall data are for the 24 hour period prior to 09:00 LT on the listed day. The four pairs of Australian stations have operated continuously throughout the study period (i.e., without being moved to a different location).

Data for Mexico and Guatemala were obtained from the Mexico Forest Fire Information System operated by the Canadian Forest Service at the Northern Forestry Centre. Weather data is collected in near real time from stations operated by the meteorological offices of the respective countries and supplying observations through the WMO's Global Observing Program and Global Telecommunications Service. The closest pairs of stations with the best observation records were chosen for this study, which were Mexicali and Tijuana in northwestern Mexico and Huehuetenango and Guatemala City Aurora in Guatemala.

For regions when no direct agency FWI System input data were available, we obtained raw hourly weather data directly from the NOAA National Climatic Data Center (NCDC) Integrated Surface Database (ISD) [Smith et al., 2011]. In many cases for the ISD stations, there were large periods of missing data. Missing values were filled with those from MERRA for the sake of being able to continue the calculations. Periods with too much missing station data over an antecedent period, however, were excluded from our monthly climatological means and comparison. We required that 80% of the previous 120 days had precipitation reporting for at least 18 hours per day. This allowed us to make use of the precipitation reported as both daily and hourly totals, but with an effort to avoid introducing a systematic bias due to missing precipitation reports. The start and end years in Table 1 indicate the full period over which some data were available, but in most case the actual periods included when comparing the DC to the gridded datasets were much shorter, often only a few years. Stations in southern Europe tended to have higher quality from the mid 2000s onward, for example, whereas data from Indonesia was typically only of sufficient quality in the mid 1990s. The comparisons with the gridded calculations take this into account, but we ~~make~~ therefore make comparisons between stations with a fair degree of caution. Information on data quality for the NCDC stations is provided as part of the dataset.

4. Results

We used the Drought Code for our comparison between station and gridded calculations because it will most directly capture the sensitivity to different precipitation input datasets. In the following section we present DC comparisons for North America, Central and South America, Northern Europe and Siberia, Southern Europe, Thailand, Malaysia and Indonesia, and Australia. This is followed by a brief description of Global FWI patterns for January and June.

4.1. North America

Figure 2 shows the monthly mean DC for three regions in Canada, for each of the three gridded datasets and two weather stations, and for northwestern Mexico. The Southern British Columbia (BC) interior DC captures the southern, drier part of Canada's Montane Cordillera ecozone [Stocks et al., 2002]. Fires in this region are numerous but tend to be smaller [Jiang et al., 2010], more often caused by humans and subject to intense fire management due to relatively high population density compared to other forested regions of the country. The DC values between the two stations are consistent for the station-based calculations, peaking in September with values approaching DC=450 (Figure 2a). The DC seasonality is captured well by the MERRA and CPC-based calculations, but has a low bias for the SHEFF precipitation, the DC for which peaks closer to DC=350. Presumably this is because of the lower spatial resolution CRU/NCEP reanalysis-based estimates used in SHEFF and the influence of weather stations on the much wetter west coast.

Large (> 200 ha) fires occur most frequently in Canada in the Boreal Shield West ecozone [Stocks et al., 2002]. Using our startup definition, the DC fire season starts in April (Figure 2b), one month later than in British Columbia. Both stations are located in Manitoba, in the western portion of the ecozone. The DC peaks in August-September between DC=250 and 300, reflecting the net drying that occurs in deeper fuels over the summer. The MERRA only-based DC (blue line) has a slightly higher bias than the SHEFF or CPC based DC relative to the station-based calculations, but all gridded DC calculations peak within the DC=300-425 danger class for that region during August and September, consistent with long-term CWFIS estimates. For reference, Amiro et al. [2004] determined that the maximum DC in this region calculated over days with large (> 200 ha) fires only was over DC=400 during September. The lower DC values in the Boreal Shield East ecozone (Figure 2c) compared to the Boreal Shield West values are consistent with a lower burned area. In the Boreal Shield West ecozone, an estimated 0.761% percent of the forested area burns annually compared to 0.145% in the Boreal Shield East ecozone [Stocks et al., 2002]. This is presumably due to the influence of large-scale, cyclonic precipitation originating in the southern US which rarely arrives to in the Boreal Shield West, and appears to have a slightly stronger influence on the Val-D'or station which is to the east of Earlton. The spread between the MERRA, SHEFF and CPC-based DC calculations is comparable to the differences between the two stations.

The stations in Mexico capture the DC condition toward the southern extent of North America (Figure 2d). Tijuana is a coastal city with a Mediterranean climate, separated by a low mountain range from Mexicali, which is on the western edge of the Sonoran desert. This arid environment has fuels similar to those found in the San Diego area in southern California [Minnich and Chou 1997], consisting of areas of chaparral and grassland in the mountains, and some broadleaf trees in the intermittent riparian zones. Fires are generally smaller on the Mexican side of the border compared to the California side, possibly in part due to differences in suppression programs [Minnich and Chou, 1997]. Over 1920-1971, for example, the mean fire size in Chamise chaparral of California was 921 ha compared to 101 ha in the same vegetation type in Mexico [Minnich and Chou, 1997]. Mexicali ~~(75 mm annually)~~ is a much drier location than Tijuana ~~(230 mm annually)~~, with the maritime influence in Tijuana providing heavier winter precipitation. Summer convective monsoon thundershowers provide Mexicali with light but regular rainfall from later summer through the early part of the winter. Due to the aridity of this environment, DC values routinely exceed DC=1000, and often reach DC=1500 in the hottest and driest summer periods. During the wetter seasons, the DC values are usually reduced to the DC=700-800 range in Mexicali and DC=300-500 in the coastal Tijuana area. The absence of winter snow or a strong wet season means that, on average, deep fuel moisture does not fully recharge and the DC does not 'zero-out'. The MERRA data generally has the highest DC values, although all model variations closely follow the DC trends in the hot and dry late summer and early autumn period. The CPC and SHEFF DC are lower than either station during the spring.

4.2. Central and South America

The stations in Guatemala capture seasonally-wet conditions in Central America (Figure 3a). Huehuetenango and Guatemala City fall in the Tropical Mountain ecological zone at similar elevations roughly 100 km inland from the Pacific Ocean. Trees are diverse and include oak, cypress, pine, and fir [Veblen, 1978]. Most fires appear to be human-caused due to agricultural slash and burn practices or escaped trash burns [Monzón-Alvarado et al., 2012]. The fire problem intensifies with deadfall left from pine beetle infestations [Billings et al., 2004]. About 90% of the annual rain falls between May and October, with slightly higher temperatures during the dry season from February through June. The Huehuetenango area receives slightly more annual precipitation (~1500 mm), with an increasing gradient up the escarpment to the north, than Guatemala City (~1200mm). The DC should therefore range from high winter values to near-zero through the summer and early fall. This trend is shown by the station and gridded data, with the mean March DC approaching DC=500 at Guatemala City at the end of the dry season. MERRA and SHEFF DC generally fall in between the two stations during the entire year. The CPC DC is consistently higher than the drier Guatemala City DC. This difference is greatest during May and June, perhaps because the CPC data are not capturing spotty, convective precipitation during the onset of the monsoon.

The Brazilian Mato Grosso is an important region of seasonal fire activity resulting from agricultural burning [Morton et al., 2013]. The peak DC approaching DC=500 (Figure 3b) is similar to the Guatemalan stations, but with opposite seasonality, peaking in August and September at the end of the dry season~~ (Figure 2)~~. The SHEFF and CPC DC are in close agreement with the station data. The MERRA DC, however has an extreme high bias, reaching peak DC=~~DC of ~~1500 and a minimum of DC=750. This reflects a strong low precipitation bias in the MERRA precipitation relative to gauge-based estimates [Lorenz and Kunstmann, 2012] that is strong enough to maintain extreme DC throughout the year.

4.3. Northern Europe and Siberia

The DC seasonality of the boreal forest region in northern Europe and Siberia (Figure 4) are similar to those of the Canadian boreal region, the Boreal Shield West especially. Peak DC values occur in September after most seasonal fuel drying has occurred and decreases as autumn progresses with decreasing environmental drying conditions. The fire season in Siberia ends in October, earlier than the other regions, due to the earlier arrival of snow. Although the range of fire weather conditions in northern boreal Eurasia is similar to boreal North America, the continental fire regimes have important differences [de Groot et al., 2013]. In comparing large fire characteristics, those in~~Fires in~~ boreal North America ~~are very large~~had a mean size of 5930 ha compared to 1312 ha in Boreal Russia, but a fire return interval of 179.9 years compared to 52.9 years in Boreal Russia.~~, infrequent, high intensity crown fires while those in boreal northern Eurasia are usually not as large, relatively frequent, and surface fires of moderate to high intensity~~ [de Groot et al. 2013b]. Divergent continental boreal fire regimes are attributed to differences in tree species even though *Picea, Pinus, Larix, Abies, Populus* and *Betula* spp. occur throughout the circumpolar boreal region [de Groot et al. 2013b]. The boreal fire regime of northern Europe and Russia east of the Urals is similar to the southern boreal of Canada with many fires being human-caused but small in size due to population size, extensive suppression capacity and road access [Lehsten et al., 2014]. There is generally fair agreement between the datasets, save for anomalously high peak MERRA DC over Germany (Figure 4c), which is consistent with Lorenz and Kunstmann's [2012] identification of lower precipitation over Central Europe in MERRA relative to gauge-based datasets.

4.4. Southern Europe

The stations in Northwestern Spain and Northern Italy form a transect across the northern Mediterranean and the stations in Southern Spain and Greece across the southern Mediterranean (Figure 5). In the Mediterranean the DC does not reflect the moisture conditions of deep soil organic layers, as soils are typically poor and a deep organic layer is normally absent [Chelli et al., 2014]. Instead, we interpret the DC as a general indicator of seasonal drying. Some studies found DC to correlate with live fuel moisture content of Mediterranean shrubs [e.g., Castro et al. 2003; Pellizzaro et al. 2007; Chelli et al., 2014]. In this case, increases in DC above 600-800 are likely not reflecting an actual increase in fire danger because the fuels have become as dry as possible. This is also likely the case in other semi-arid regions.

Northwestern Spain has a marked Atlantic climate with the highest precipitation amount in the Iberian Peninsula. Atmospheric circulation in the summer is highly variable, alternating between strong dry and humid periods [Garcia Diez, 1993]. It is one of the more fire prone regions in Spain [Padilla & Vega-Garcia 2011] with ~~an extremely high number of fires~~ ~6000 fires per year, typically concentrated during short dry summer periods. Total burned area is ~~also high but~~ ~30 000 ha per year, but the ~~average~~mean fire size of 4.9 ha is less than in the rest of Spain (7.6 ha) due to aggressive suppression policy [Padilla and Vega-Garcia, 2011]. Extremely large (> 500 ha) fires ~~are rare~~ constitute only 0.13% of all fires, but fire-fighting agencies are often challenged by many fires burning at the same time [Padilla and Vega-Garcia, 2011]. Fire occurrence patterns are affected more by human activities than by biophysical characteristics of the fire environment [Padilla and Vega-Garcia, 2011], but there is an August peak in fire activity. The DC peaks in September (Figure 5a), and is higher at La Coruna (DC=500) on the coast compared to Santiago located 50km inland. The CPC and SHEFF DC fall in between the two stations, with MERRA being slightly higher throughout the year.

The stations in Southern Spain capture a typical inland Mediterranean climate with dry hot summers. The vegetation is dominated by a mosaic of shrublands and low forests with frequent crown-fires [Keeley et al., 2011]. Although this is a fire prone area and large fires may occur, fire activity is less remarkable than in other Mediterranean regions [Pausas and Paula, 2012] with 900 fires each year, having a mean size of 13.5 ha and total annual average area burned of 12 000 . In the extremely dry climatic condition of the area, fuel structure tends to be more relevant in driving fire activity than the frequency of climatic conditions conducive to fire [Pausas and Paula, 2012]. Wildfires are more fuel-limited and more extreme climatic conditions (higher aridity than in more mesic regions) are needed for fires to spread successfully [Pausas and Paula, 2012]. The peak of the fire season is typically in June, July, August, corresponding to ~~DC~~ values between DC=500 and 1000 (Figure 5b). The DC seasonality and magnitude at the Seville and Cordoba stations are essentially identical, with both stations in the low-lying Guadalquivir river basin. All gridded data slightly overestimate DC in summer months, and the MERRA DC is slightly higher throughout the year.

The stations in Northern Italy south of the Alps reflect a sub-continental temperate climate, with predominantly deciduous broadleaved forest [Zumbrunnen et al. 2009, Wastl et al 2013]. The peak of the fire activity is in March-April, after snowmelt and before leaf flushing. Population, vegetation phenology and short-term dryness of surface soil layers often triggered by Foehn winds off the Alps are the main drivers, rather than long term DC. Fires in this region are on average small, with mean fire size ~2 ha and 98% of fires smaller than 10 ha, and rarely achieve crown involvement [Zumbrunnen et al. 2009, Wastl et al., 2013]. The station and gridded data are all similar, peaking at the end of the summer near DC=500 (Figure 5c).

The stations in Greece reflect a Mediterranean climate, but one less arid than Southern Spain and one with severe fire incidence and frequent large fires during the summer. 1.2 % of fires are larger than 500 ha and the average fire size is 45 ha. DC peaks in August September with extremely high values approaching DC=1000, slightly lower at Aktion due to its coastal location 100km to the north (Figure 5d). SHEFF and CPC are in good agreement with Andravida weather station and MERRA has a high DC bias throughout the year. Seasonal drought is an important driver of fire activity in the area, but as in the rest of the Mediterranean region, the deep organic layer of soil is absent in most cases, thus DC reflects seasonal drying rather than moisture content of deep organic fuels. Significant relationships of monthly burned area and FWI components (DC and ISI), were found for the Mediterranean region [Camia and Amatulli, 2009] and for individual southern European countries including Greece [Amatulli et al., 2013].

4.5. Thailand

The fire season in Thailand is from early December to early May during the southward displacement of the Inter-tropical Convergence Zone (ITCZ) [Tanpipat et al., 2009; Chien et al., 2011]. Fires are usually human-caused for the purposes of gathering non-timber products, hunting and agriculture, and occur primarily in the afternoon [Tanpipat et al., 2009; Chien et al., 2011]. Thailand is an important region for possible FWI System use given the persistence of its fire and haze problem and the expanding role of the Association of Southeast Asian Nations (ASEAN) for fire management, to which the FWI System is central [de Groot et al., 2007].

Figure 6 shows monthly mean DC for two regions in Thailand. Biomass burning is the dominant emissions source for particulate matter in northwest Thailand [Nguyen and Leelasakultum, 2011], which experiences periodically severe haze as a result. The DC peaks in March and April at both stations, followed by the end of the dry season (Figure 6a). In Chiang Mai, there is also a secondary dry period in July, but its absence in Chiang Rai suggests local effects or artefacts of input data common to both gridded precipitation datasets. The minimum DC in both locations occurs in the August to September period during the height of the Asian summer monsoon. The SHEFF and CPC-based DC are in good agreement with station data for both locations, both falling between the two stations during most of the year. There is a strong low DC bias in the MERRA dataset throughout the year. The DC in northeast Thailand (Figure 6b) has roughly the same seasonality, but with a higher March peak. The CPC, SHEFF and station-based DC are all in strong agreement, and the MERRA-based DC again shows a low bias. Compared to northwest Thailand, there is a smaller difference between the two stations in the northeast, which we attribute to the region's uniform topography.

4.6. Malaysia and Indonesia

The stations in Malaysia and Indonesia are representative of the Equatorial Southeast Asia fire region identified by van der Werf et al. [2010]. Fire activity in southern Sumatra and southern Kalimantan is higher than in Sabah or Peninsular

Malaysia [van der Werf et al., 2008; Langner & Siegert, 2009; Giglio et al., 2013]. On the average, close to 5% of these Indonesian regions burn per year, while the comparable statistic for these Malaysian regions is less than 0.3% [Giglio et al., 2013]. This is due to greater forest loss over the past two decades in Indonesia, principally due to deforestation fires for establishing palm oil, timber and pulp paper plantations, as well as escaped fires linked to illegal logging activities [Langner & Siegert, 2009; Mukherjee & Sovacool, 2014]. These fires have left many areas with highly degraded forests that are prone to even more fires, especially during El-Niño events [Hoscilo et al. 2011]. These problems are mitigated in Malaysia to some extent by more active monitoring, regulation and enforcement by government authorities and fire suppression [Langner & Siegert, 2009; Forsyth, 2014; Mukherjee & Sovacool, 2014] compared with Indonesia. The fire seasons in the region are controlled by rainfall seasonality. Distinct regions of the Maritime Continent that have an annual wet-dry cycle, a semi-annual cycle or that have no clear rainy and dry seasons [Aldrian and Susanto, 2003]. In southern Sumatra and southern Kalimantan, the monsoon consists of two distinct phases with the wet season occurring in the early part of the year (January-March) and the dry season in the middle of the year (July-September) [Aldrian and Susanto, 2003].

The seasonal DC patterns for Peninsula Malaysia, Sabah, southern Sumatra, and southern Kalimantan (Figure 7) reflect these rainfall patterns. Southern Sumatra has the strongest DC seasonality (Figure 7c); the longer dry season allows mean DC approaching 300 to be reached in September. The timing and magnitude are well captured by the SHEFF and CPC datasets, but a wet MERRA bias results in lower DC. The seasonality in Southern Kalimantan is similar (Figure 7d), but on average, the peak DC of DC=200 is lower than Sumatra.

The DC seasonality in Malaysia is less consistent than Indonesia. In Peninsular Malaysia (Figure 7a), both stations have a July peak, but which is higher at KLIA compared to Petaling Jaya, perhaps reflecting localized effects. The CPC DC corresponds closely to that in Petaling Jaya, and MERRA has very little seasonality. In Sabah (Figure 7b), there is a strong DC seasonality in Kota Kinabalu, but not in Sandakan. The difference is likely due to complex air-sea interaction and topography, with the two stations separated by the Crocker mountain range. The more complicated seasonality in Malaysia reflects the fact that it falls outside of the distinct rainfall zone identified by Aldrian and Susanto [2003]. We note, however, that the apparently strong differences between datasets reflect a narrower DC scale and should not be over-interpreted.

El-Niño induced droughts are a recurrent feature of the region, and hence, inter-annual variability in rainfall across the regions is high [van der Werf et al., 2008; Field et al., 2008; Field et al., 2009; Spessa et al., 20154]. As such, there is considerable variation surrounding the long-term ~~average~~mean monthly DC values shown in Figure 7. Field et al. [2004] estimated that the severe fire episodes in 1994 and 1997 in Sumatra and Kalimantan were associated with DC greater than DC=400.

During non-El Nino years, and on average, this DC threshold is not reached and heavy fuels, especially peat, remain too moist to burn.

Viewed regionally across Southeast Asia, the DC seasonality in Indonesia is opposite that of Thailand, with Malaysia falling in between. MERRA-derived DC is consistently lower than all DC products in all regions, especially during the dry season. This is similar to Thailand, and consistent with previous work showing that MERRA has a wet bias in Southeast Asia relative to gauge-based estimates [Lorentz and Kunstmann, 2012].

4.7. Australia

Monthly mean DC values are shown in Figure 8 for four regions in Australia. In Western Australia (Figure 8a), the seasonal cycle of the DC values based on the gridded data is similar to that of the station-based data in that maximum values occur during the warmer months and the minimum values during the cooler months. The DC values based on the Esperance station data are lower than those based on the Kalgoorlie-Boulder station data, with a maximum approaching DC=700 in March and a minimum of DC=100 in September. This is consistent with Esperance being located nearer to the coast with a cooler and wetter climate than Kalgoorlie-Boulder, where the August minimum is DC=500. The DC values based on the gridded data are similar in magnitude to those based on the more inland station (Kalgoorlie-Boulder), with DC values based on SHEFF and CPC data being highly consistent throughout the year with the Kalgoorlie-Boulder station-based data. The DC values based on MERRA are somewhat higher than the Kalgoorlie-Boulder station-based data during the cooler months of the year, and relatively similar to the other two gridded data sets during the warmer months of the year.

In the Northern Territory (Figure 8b), the DC values based on the Tennant Creek station data have a maximum approaching DC=1000 during spring (from about September to November) corresponding to the later part of the tropical dry season in the Southern Hemisphere. The DC values based on the Alice Springs station data have a less pronounced seasonal cycle than the case for Tennant Creek, due to Alice Springs being located somewhat further south and having a more temperate climate than Tennant Creek. The DC values based on the gridded data have magnitudes broadly similar to the station-based data with a seasonal cycle similar to the case for Tennant Creek (i.e. a more pronounced spring maximum than the case for Alice Springs). There is little variation between the three gridded datasets for any month of the year.

In New South Wales (Figure 8c), the gridded data are consistent with the station data in having maximum DC values during the warmer months of the year. The DC values based on the gridded data tend to be larger in magnitude than those based on the station data. This is consistent with the gridded data representing the ~~average~~mean conditions throughout a grid cell, whereas the two stations are both located very close to the coast and have relatively moderate temperatures and high rainfall as compared to nearby inland regions.

In Victoria (Figure 8d), the DC values based on the data from the two stations are very similar to each other throughout the year, peaking at DC=600 in March. These stations are located relatively close to each other and both have strong maritime influences on their climate. The DC values based on the SHEFF and CPC data are almost identical to those based on the station data for all months of the year. The DC values based on MERRA data capture the seasonal cycle, but are consistently higher by DC=200.

Regional fire activity in Australia broadly follows the timing of the seasonal cycle of DC values shown in Figure 8. In Victoria, fire activity predominantly occurs during the warmer months of the year, with a peak in fire activity around the later parts of summer from about January to March, while noting that occasional serious fires are likely to occur anytime from about November to April [Luke and McArthur, 1978; Russell-Smith et al., 2007]. For example, the fire affected region during the January to March period is on average about 0.41% of the south-eastern mesic region of Australia, compared with only about 0.03% from April to June, 0.05% from July to September and 0.11% from October to December [Russell-Smith et al., 2007]. The DC values for the Victorian stations peak from February to April, indicating considerable overlap with the period of peak fire activity in this region as well as a tendency towards a time lag of about one month compared to the timing of fire activity. This time lag could be expected to some degree given that the fuel drying speed indicated by the DC is about 52 days (i.e. the time to lose about two thirds of its free moisture above equilibrium), as compared to about 12 days for the DMC and 2/3 of a day for the FFMC, with the FFMC and DMC also being important indicators of severe fire weather conditions in Australia in addition to the DC [Dowdy et al., 2010].

4.8. Summary of DC comparisons

Over northern latitudes with winter shutdown (Montane Cordillera, Boreal Shield West, Boreal Shield East, Sweden, Finland, Germany and Siberia), DC peaks in August and September between DC=200 and 500. Mediterranean regions showed the same seasonality, but for in Southern Spain and Greece, the hottest regions considered, values exceeded DC=1000 depending on the dataset. DC values across datasets diverged over the course of the summer from similar, low startup values, but no systematic differences were apparent across different datasets, except perhaps that the DC calculations based on SHEFF tended had lower peak values in the Montane Cordillera, Boreal Shield East and Sweden and Siberia.

Regions in Australia exhibited the weakest DC seasonality. In Western Australia and the Northern Territory, values ranged between DC=500 and 1000, never, on average, 'bottoming-out'. DC values were lower in New South Wales and Victoria, but also not, on average, reaching 0, which was the case for the two stations presumably due to their coastal location.

Guatemala, the Brazilian Mato Grosso and Thailand have the strongest wet-dry seasonality. Excluding MERRA, DC peaked between DC=400 and 600 and approached 0 during the wet season. The lowest overall values were in Equatorial Southeast Asia which lacks as pronounced a dry season. The Malaysian regions lacked pronounced seasonal maxima and the gridded products never exceeded seasonal means of DC=100. The Indonesian regions had a greater seasonality, but with seasonal peaks of less than DC=300. As stated above, this seasonal average masks strong interannual variability.

4.9. Global FWI variability

~~Figure 8 shows the mean May snow depth and fraction of days over which the FWI System is active, based on our startup and shutdown procedures. The maps essentially show the dependence and variability of FWI System startup on snow cover, in this case estimated from MERRA.~~

Figure 9 shows the mean, global Fire Weather Index (FWI) during January and July for all three datasets. The mean FWI is calculated from 1980-2012 ~~onwards~~, excluding 1979 as a moisture code equilibration year. We describe FWI seasonality according to selected fire regions defined by van der Werf et al. [2010], starting with the MERRA-based calculations. In January, FWI calculations are not active over the Boreal North America and Boreal Asia regions. Over Temperate North America and Europe, mean FWI values reflect only a small number of anomalous warm and snow-free days during which the calculations were active. At low latitudes, the highest values based on MERRA are over Northern Hemisphere Africa, which contributes significantly to global emissions, when the ITCZ is displaced to the south. FWI is also high (> 40) in areas of Southern Hemisphere South America, the southern half of Australia, excepting its eastern coast, and northwest India. There are moderate (20-40) FWI values in Mexico and parts of continental Southeast Asia. Elsewhere, the FWI is generally low, including over the Amazon basin, Northern Hemisphere South America, the Congo basin, and Equatorial Southeast Asia.

In June, the FWI System is active over the northern Boreal regions, and does generally not exceed 30. Although an FWI of 30 is well below the seasonal peak at low latitudes, this can reflect severe fire danger conditions over the boreal regions. In the northern temperate regions, high values are seen over the fire prone regions of the western US (approaching 50) and the Mediterranean. The extremely high FWI over Northern Hemisphere Africa has mostly been replaced by low FWI during the wet season and onset of the West African monsoon. By July, the dry season in Equatorial Southeast Asia has just started and FWI values are still low. High FWI values are seen in Southern Hemisphere South America, corresponding, for example, to the active fire season in the Brazilian Mato Grosso [Chen et al., 2011; Fernandes et al., 2011], with comparable increases over southern Africa and northern Australia, all corresponding to the northward shift of the ITCZ.

In Australia, the three gridded data sets show strong similarities to each other in most regions during January and July. The highest FWI values during January tend to occur in the southern and southwestern regions, due to the dry and hot summer conditions of the temperate climate, while during July the highest values occur in the northern regions corresponding to the tropical dry season. The FWI values in eastern Australia are generally not as high as in other parts of mainland Australia, consistent with previous studies based on numerical weather prediction (NWP) analyses [Dowdy et al., 2010], relating to the significant maritime influences that occur in this region (e.g. trade wind transport of moist air inland from the Pacific Ocean).

Viewed globally, there is strong agreement between the three datasets. All major seasonal differences in the MERRA FWI are present in the SHEFF and CPC FWI. In January, the strongest difference was over central South America, where SHEFF and in particular CPC FWI were much lower than MERRA. This is consistent with the strong low precipitation bias in MERRA over the region identified by Lorenz and Kunstmann [2012], and effect on the DC described previously. SHEFF and CPC FWI are higher over Mexico, Northern Hemisphere Africa, continental Southeast Asia and northern Australia. In June, the higher MERRA values persist, but with an eastward shift. Sheffield and CPC FWI tended to be higher over the southeast US, East Africa and Southern India.

The consistency in the differences between MERRA and the two gauge-based FWI calculations reflects the common station data used in computing the latter two. Whether or not the gauge-based calculations are better will ultimately depend on the underlying rain gauge density. This information was available for the CPC precipitation dataset, shown in Figure 10 during the 1979-2012 period. Values less than 1 indicate stations not operating during the full analysis period. Users are encouraged to consider rain gauge density for any region over which analyses are performed.

Globally, gauge density is highest over the US, eastern Brazil and the populated coastal regions of Australia. Density is reasonably high over central South America, which suggests that the low bias in the MERRA precipitation is genuine and that the MERRA FWI values there are unreliable. This is likely the case for MERRA's high precipitation and low FWI biases over continental Southeast Asia also, or for Thailand at least, where the CPC station density is high. In the northern Boreal region, coverage is sparse but fairly even across fire prone areas. In Southeast Asia, rain gauge density is low over the severe burning regions of Borneo and Sumatra. This limits spatially-detailed FWI analysis over the region, although previous analyses have shown that precipitation covariance over the region is strong enough [Aldrian and Susanto, 2003] that the FWI System values should provide useful information at a provincial or state-level. Identifying a more appropriate FWI version over tropical Africa is difficult due to the sparse and uneven gauge distribution, as cautioned by Chen et al. [2008] for precipitation-based analyses in general.

5. Summary

We have developed a global database of the Canadian FWI System components using MERRA reanalysis and two different gauge-based precipitation datasets. This dataset can be used for historical relationships between fire weather and fire activity at continental and global scales, in identifying large-scale atmosphere-ocean controls on fire weather, calibration of FWI-based fire prediction models, and as a baseline for projections of fire weather under future climate scenarios as the reanalysis products improve.

Compared to the station-based calculation, the strongest differences between the three datasets occurred for the MERRA-based DC calculations at low-latitudes. These biases were in either direction: over the Mato-Grosso peak dry season DC was higher than station or gridded rain gauge calculations by a factor of three, but, conversely had a low bias over Southeast Asia. We attribute these biases to the inherent difficulty in modelling convective precipitation, which remains a central challenge to numerical weather and climate modelling [Arakawa, 2004], and has disproportionate effects over the tropics. Temperature, wind and humidity discrepancies could also be contributing to the differences between gridded and station based calculations, particularly over regions with significant topography. While we have examined only one reanalysis-based product, we argue that FWI System calculations based solely on reanalysis products will be subject to the same discrepancies, and that alternative precipitation estimates are important to consider. Users are encouraged to conduct analyses over all three precipitation-based datasets.

In the future, we hope to increase the number of versions using other input datasets, for example, other state-of-the-art reanalyses or satellite-based precipitation estimates such as Global Precipitation Climatology Project (GPCP) [Huffman et al., 2009], Tropical Rainfall Measuring Mission (TRMM) [Huffman et al., 2007] and Global Precipitation Measurement (GPM) [Smith et al., 2007]. There is also the potential to compute the moisture codes using new soil moisture retrievals from the Soil Moisture and Ocean Salinity Mission (SMOS) [Kerr et al., 2010] and Soil Moisture Active Passive (SMAP) [Entekhabi et al., 2010] missions. The datasets could also be extended to include other weather-based fire danger indices such as the Nesterov Index, which continues to be used operationally and for research purposes [Thonicke et al., 2010] the McArthur Forest Fire Danger Index [McArthur, 1967; Nobel et al., 1980], and, to capture the influence of atmospheric instability, the Haines Index [Haines, 1988]. In regions with seasonal snow cover, different moisture code startup procedures and snow cover estimates should be examined, ideally taking into account local land cover and topographic characteristics. We hope that users of the data continue to compare gridded fire weather calculations against those from weather stations, particularly for regions not considered here, and from secondary meteorological networks not used in any of the MERRA, Sheffield or CPC datasets. We also encourage comparison for components other than the DC, especially the ISI and FWI which are strongly influenced by surface winds.

Data access

All data and code used in generating GFWED can be obtained from http://data.giss.nasa.gov/impacts/gfwed/.

Acknowledgements

We thank Jose Moreno and an anonymous reviewer for their short comment and detailed review, respectively. We thank Steve Taylor for his review and for identifying and pointing out the error in DMC lag times. VT and KM thank the Thailand Meteorological Department for providing weather data, and Prayoonyong Nhuchaiya for guidance. AD was supported by the Australian Climate Change Science Program (ACCSP). AS is supported by the Open University Research Investment Fellowship scheme. Resources supporting this work were provided by the NASA High-End Computing (HEC) Program through the NASA Center for Climate Simulation (NCCS) at Goddard Space Flight Center.

Table of acronyms

Acronym	Definition
ASEAN	Association of Southeast Asian Nations
BUI	Buildup Index
CFS	Canadian Forest Service
CPC	Climate Prediction Center precipitation (Chen et al., 2008)
CRU	Climate Research Unit
CWFIS	Canadian Wildland Fire Information System
DC	Drought Code
DMC	Duff Moisture Code
DSR	Daily Severity Rating
EnvCan	Environment Canada
FFMC	Fine Fuel Moisture Code
FWI	Fire Weather Index
GPM	Global Precipitation Measurement
ISI	Initial Spread Index
ITCZ	Intertropical Convergence Zone
KLIA	Kuala Lumpur International Airport
LT	Local time
MERRA	Modern Era Retrospective ReAnalysis (Rienecker et al., 2011)
MODIS	Moderate Resolution Imaging Spectroradiometer
NCAR	National Center for Atmospheric Research
NCDC ISD	National Climatic Center Integrated Surface Database
NCEP	National Center for Environmental Prediction
NOAA	National Oceanic and Atmospheric Admininstration
NWP	Numerical Weather Prediction
QuickScat	Quick Scatterom~~o~~eter
SHEFF	Sheffield precipitation (Sheffield et al., 2006)
SMAP	Soil Moisture Active Passive
SMOS	Soil Moisture Ocean Salinity

SSM/I	Special Sensor Microwave Imager
TRMM	Tropical Rainfall Measuring Mission
UEA	University of East Anglia
WMO	World Meteorological Organization

References

Aldrian, E., and R. D. Susanto (2003), Identification of three dominant rainfall regions within Indonesia and their relationship to sea surface temperature, *International Journal of Climatology*, *23*(12), 1435-1452, doi:10.1002/joc.950.

Alexandersson, H. (1986), A homogeneity test applied to precipitation data, *Journal of Climatology*, *6*(6), 661-675.

Amatulli, G., A. Camia, and J. San-Miguel-Ayanz (2013), Estimating future burned areas under changing climate in the EU-Mediterranean countries, *Science of the Total Environment*, *450*, 209-222, doi:10.1016/j.scitotenv.2013.02.014.

Amiro, B. D., K. A. Logan, B. M. Wotton, M. D. Flannigan, J. B. Todd, B. J. Stocks, and D. L. Martell (2004), Fire weather index system components for large fires in the Canadian boreal forest, *International Journal of Wildland Fire*, *13*(4), 391-400, doi:10.1071/wf03066.

Arakawa, A. (2004), The cumulus parameterization problem: Past, present, and future, *Journal of Climate*, *17*(13), 2493-2525, doi:10.1175/1520-0442(2004)017<2493:ratcpp>2.0.co;2.

Bedia, J., S. Herrera, J. M. Gutierrez, G. Zavala, I. R. Urbieta, and J. M. Moreno (2012), Sensitivity of fire weather index to different reanalysis products in the Iberian Peninsula, *Natural Hazards and Earth System Sciences*, *12*(3), 699-708, doi:10.5194/nhess-12-699-2012.

Billings, R. F., S. R. Clarke, V. Espino Mendoza, P. Cordon Cabrera, and B. Melendez Figueroa (2004), Bark beetle outbreaks and fire: A devastating combination for Central America's pine forests, *Unasylva*, *55*(217), 15-18.

Camia, A., and G. Amatulli (2009), Weather Factors and Fire Danger in the Mediterranean, in

Earth Observation of Wildland Fires in Mediterranean Ecosystems, edited by E. Chuvieco, pp. 71-82, Springer-Verlag, Berlin, doi:10.1007/978-3-642-01754-4_6.

Camia, A., and G. Amatulli (2010), Climatology of FWI over Europe: fire danger anomalies and index percentiles rankings, in *VI International Conference on Forest Fire Research*, edited by D. Viegas, p. 12, Coimbra, Portugal.

Castro, F. X., A. Tudela, and M. T. Sebastia (2003), Modeling moisture content in shrubs to predict fire risk in Catalonia (Spain), *Agricultural and Forest Meteorology*, *116*(1-2), 49-59, doi:10.1016/s0168-1923(02)00248-4.

Chelli, S., P. Maponi, G. Campetella, P. Monteverde, M. Foglia, E. Paris, A. Lolis, and T. Panagopoulos (2014), Adaptation of the Canadian Fire Weather Index to Mediterranean Forests, *Natural Hazards*, 1-16, doi:10.1007/s11069-014-1397-8.

Chen, M. Y., W. Shi, P. P. Xie, V. B. S. Silva, V. E. Kousky, R. W. Higgins, and J. E. Janowiak (2008), Assessing objective techniques for gauge-based analyses of global daily precipitation, *Journal of Geophysical Research-Atmospheres*, *113*(D4), 13, doi:10.1029/2007jd009132.

Chen, Y., J. T. Randerson, D. C. Morton, R. S. DeFries, G. J. Collatz, P. S. Kasibhatla, L. Giglio, Y. Jin, and M. E. Marlier (2011), Forecasting Fire Season Severity in South America Using Sea Surface Temperature Anomalies, *Science*, *334*(6057), 787-791, doi:10.1126/science.1209472.

Chien, S., J. Doubleday, D. McLaren, A. Davies, D. Tran, V. Tanpipat, S. Akaakara, A. Ratanasuwan, and D. Mandl (2011), Space-based sensorweb monitoring of wildfires in Thailand, *2011 IEEE International Geoscience and Remote Sensing Symposium (IGARSS)*, 1906-1909.

Chu, T., and X. Guo (2014), An assessment of fire occurrence regime and performance of Canadian fire weather index in south central Siberian boreal region, *Natural Hazards and Earth System Sciences Discussions*, *2*, 4711-4742.

de Groot, W. J., A. S. Cantin, M. D. Flannigan, A. J. Soja, L. M. Gowman, and A. Newbery (2013a), A comparison of Canadian and Russian boreal forest fire regimes, *Forest Ecology and Management*, *294*, 23-34, doi:10.1016/j.foreco.2012.07.033.

de Groot, W. J., and M. D. Flannigan (2014), Climate Change and Early Warning Systems for Wildland Fire, in *Reducing Disaster: Early Warning Systems for Climate Change*, edited by Z. Zommers and A. Singh, pp. 127-151, Springer, Dordrecht, doi:10.1007/978-94-017-8598-3.

de Groot, W. J., M. D. Flannigan, and A. S. Cantin (2013b), Climate change impacts on future boreal fire regimes, *Forest Ecology and Management*, *294*, 35-44, doi:10.1016/j.foreco.2012.09.027.

de Groot, W. J., J. G. Goldammer, T. Keenan, M. A. Brady, T. J. Lynham, C. O. Justice, I. A. Csiszar, and K. O. Loughlin (2006), Developing a global early warning system for wildland fire, in *V International Conference on Forest Fire Research*, edited by D. Viegas, p. 12, Coimbra, Portugal.

Diez, E. L. G., J. L. L. Salazar, and F. D. Davila (1993), Some meteorological conditions associated with forest-fires in Galicia (Spain), *International Journal of Biometeorology*, *37*(4), 194-199.

Dowdy, A. J., G. A. Mills, K. Finkele, and W. de Groot (2010), Index sensitivity analysis applied to the Canadian Forest Fire Weather Index and the McArthur Forest Fire Danger Index, *Meteorological Applications*, *17*(3), 298-312, doi:10.1002/met.170.

Dowdy, A. J., G. A. Mills, K. Finkele, and W. J. de Groot (2009), Australian fire weather as represented by the McArthur Forest Fire Danger Index and the Canadian Forest Fire Weather Index*Rep.*, 84 pp, Centre for Australian Weather and Climate Research.

Entekhabi, D., et al. (2010), The Soil Moisture Active Passive (SMAP) Mission, *Proceedings of the Ieee*, *98*(5), 704-716, doi:10.1109/jproc.2010.2043918.

Fernandes, K., et al. (2011), North Tropical Atlantic influence on western Amazon fire season variability, *Geophysical Research Letters*, *38*, doi:10.1029/2011gl047392.

Field, R. D., and S. S. P. Shen (2008), Predictability of carbon emissions from biomass burning in Indonesia from 1997 to 2006, *Journal of Geophysical Research-Biogeosciences*, *113*(G4), 17, doi:10.1029/2008jg000694.

Field, R. D., G. R. van der Werf, and S. S. P. Shen (2009), Human amplification of drought-induced biomass burning in Indonesia since 1960, *Nature Geoscience*, *2*(3), 185-188, doi:10.1038/ngeo443.

Field, R. D., Y. Wang, O. Roswintiarti, and Guswanto (2004), A drought-based predictor of recent haze events in western Indonesia, *Atmospheric Environment*, *38*(13), 1869-1878, doi:10.1016/j.atmosenv.2004.01.011.

Flannigan, M., A. S. Cantin, W. J. de Groot, M. Wotton, A. Newbery, and L. M. Gowman (2013), Global wildland fire season severity in the 21st century, *Forest Ecology and Management*, *294*, 54-61, doi:10.1016/j.foreco.2012.10.022.

Forsyth, T. (2014), Public concerns about transboundary haze: A comparison of Indonesia, Singapore, and Malaysia, *Global Environmental Change-Human and Policy Dimensions*, *25*, 76-86, doi:10.1016/j.gloenvcha.2014.01.013.

Giglio, L., J. T. Randerson, and G. R. van der Werf (2013), Analysis of daily, monthly, and annual burned area using the fourth-generation global fire emissions database (GFED4), *Journal of Geophysical Research-Biogeosciences*, *118*(1), 317-328, doi:10.1002/jgrg.20042.

Haines, D. A. (1988), A lower atmospheric severity index for wildland fires, *National Weather Digest*, *13*(3), 23-27.

Horel, J., R. Ziel, C. Galli, J. Pechmann, and X. Dong (in press), An evaluation of Fire Danger and Behaviour Indices in the Great Lakes Region Calculated from Station and Gridded Weather Information, *International Journal of Wildland Fire*, *23*(2), 202-214, doi:http://dx.doi.org/10.1071/WF12186.

Hoscilo, A., S. E. Page, K. J. Tansey, and J. O. Rieley (2011), Effect of repeated fires on land-cover change on peatland in southern Central Kalimantan, Indonesia, from 1973 to 2005, *International Journal of Wildland Fire*, *20*(4), 578-588, doi:10.1071/wf10029.

Huffman, G. J., R. F. Adler, D. T. Bolvin, and G. Gu (2009), Improving the global precipitation record: GPCP Version 2.1, *Geophysical Research Letters*, *36*, doi:10.1029/2009gl040000.

Huffman, G. J., R. F. Adler, D. T. Bolvin, G. Gu, E. J. Nelkin, K. P. Bowman, Y. Hong, E. F. Stocker, and D. B. Wolff (2007), The TRMM multisatellite precipitation analysis (TMPA): Quasi-global, multiyear, combined-sensor precipitation estimates at fine scales, *Journal of Hydrometeorology*, *8*(1), 38-55, doi:10.1175/jhm560.1.

Jiang, Y., Q. Zhuang, M. D. Flannigan, and J. M. Little (2009), Characterization of wildfire regimes in Canadian boreal terrestrial ecosystems, *International Journal of Wildland Fire*, *18*(8), 992-1002, doi:10.1071/wf08096.

Kalnay, E., et al. (1996), The NCEP/NCAR 40-year reanalysis project, *Bulletin of the American*

Meteorological Society, *77*(3), 437-471, doi:10.1175/1520-0477(1996)077<0437:tnyrp>2.0.co;2.

Keeley, J. E., W. J. Bond, R. A. Bradstock, J. G. Pausas, and P. W. Rundel (2011), *Fire in Mediterranean Ecosystems: Ecology, Evolution and Management*, 522 pp., Cambridge University Press, Cambridge.

Kerr, Y. H., et al. (2010), The SMOS Mission: New Tool for Monitoring Key Elements of the Global Water Cycle, *Proceedings of the Ieee*, *98*(5), 666-687, doi:10.1109/jproc.2010.2043032.

Langner, A., and F. Siegert (2009), Spatiotemporal fire occurrence in Borneo over a period of 10 years, *Global Change Biology*, *15*(1), 48-62, doi:10.1111/j.1365-2486.2008.01828.x.

Lawson, B. D., and O. B. Armitage (2008), Weather guide for the Canadian Forest Fire Danger Rating System*Rep.*, 73 pp, Northern Forestry Centre, Edmonton, Canada.

Lee, B. S., M. E. Alexander, B. C. Hawkes, T. J. Lynham, B. J. Stocks, and P. Englefield (2002), Information systems in support of wildland fire management decision making in Canada, *Computers and Electronics in Agriculture*, *37*(1-3), 185-198, doi:10.1016/s0168-1699(02)00120-5.

Lehsten, V., W. J. de Groot, M. Flannigan, C. George, P. Harmand, and H. Balzter (2014), Wildfires in boreal ecoregions: Evaluating the power law assumption and intra-annual and interannual variations, *Journal of Geophysical Research-Biogeosciences*, *119*(1), 14-23, doi:10.1002/2012jg002252.

Lorenz, C., and H. Kunstmann (2012), The Hydrological Cycle in Three State-of-the-Art Reanalyses: Intercomparison and Performance Analysis, *Journal of Hydrometeorology*, *13*(5), 1397-1420, doi:10.1175/jhm-d-11-088.1.

Lucas, C. (2010), On developing a historical fire weather data-set for Australia, *Australian Meteorological and Oceanographic Journal*, *60*(1), 1-13.

Luke, R. H., and A. G. McArthur (1978), *Bushfires in Australia*, 359 pp., Australia Forestry and Timber Bureau, Commonwealth Scientific and Industrial Research Organization, Division of Forest Research., Canberra.

Manomaiphiboon, K., M. Octaviani, K. Torsri, and S. Towprayoon (2013), Projected changes in means and extremes of temperature and precipitation over Thailand under three future emissions scenarios, *Climate Research*, *58*(2), 97-115, doi:10.3354/cr01188.

McArthur, A. G. (1967), Fire behaviour in Eucalyptus Forests*Rep.*, Department of National Development Forestry and Timber Bureau, Canberra.

Minnich, R. A., and Y. H. Chou (1997), Wildland fire patch dynamics in the chaparral of southern California and northern Baja California, *International Journal of Wildland Fire*, *7*(3), 221-248, doi:10.1071/wf9970221.

Mitchell, T. D., and P. D. Jones (2005), An improved method of constructing a database of monthly climate observations and associated high-resolution grids, *International Journal of Climatology*, *25*(6), 693-712, doi:10.1002/joc.1181.

Monzon-Alvarado, C., S. Cortina-Villar, B. Schmook, A. Flamenco-Sandoval, Z. Christman, and L. Arriola (2012), Land-use decision-making after large-scale forest fires: Analyzing fires as a driver of deforestation in Laguna del Tigre National Park, Guatemala, *Applied Geography*, *35*(1-2), 43-52, doi:10.1016/j.apgeog.2012.04.008.

Morton, D. C., Y. Le Page, R. DeFries, G. J. Collatz, and G. C. Hurtt (2013), Understorey fire frequency and the fate of burned forests in southern Amazonia, *Philosophical Transactions of the Royal Society B-Biological Sciences*, *368*(1619), doi:10.1098/rstb.2012.0163.

Mukherjee, I., and B. K. Sovacool (2014), Palm oil-based biofuels and sustainability in southeast Asia: A review of Indonesia, Malaysia and Thailand, *Renewable and Sustainable Energy Reviews*, *37*, 1-12.

Nguyen, T. K. O., and K. Leelasakultum (2011), Analysis of meteorology and emission in haze episode prevalence over mountain-bounded region for early warning, *Science of the Total Environment*, *409*(11), 2261-2271, doi:10.1016/j.scitotenv.2011.02.022.

Noble, I. R., G. A. V. Bary, and A. M. Gill (1980), MCARTHUR FIRE-DANGER METERS EXPRESSED AS EQUATIONS, *Australian Journal of Ecology*, *5*(2), 201-203, doi:10.1111/j.1442-9993.1980.tb01243.x.

Padilla, M., and C. Vega-Garcia (2011), On the comparative importance of fire danger rating indices and their integration with spatial and temporal variables for predicting daily human-caused fire occurrences in Spain, *International Journal of Wildland Fire*, *20*(1), 46-58, doi:10.1071/wf09139.

Pausas, J. G., and S. Paula (2012), Fuel shapes the fire-climate relationship: evidence from Mediterranean ecosystems, *Global Ecology and Biogeography*, *21*(11), 1074-1082, doi:10.1111/j.1466-8238.2012.00769.x.

Pellizzaro, G., C. Cesaraccio, P. Duce, A. Ventura, and P. Zara (2007), Relationships between seasonal patterns of live fuel moisture and meteorological drought indices for Mediterranean shrubland species, *International Journal of Wildland Fire*, *16*(2), 232-241, doi:10.1071/wf06081.

Reynolds, R. W., N. A. Rayner, T. M. Smith, D. C. Stokes, and W. Q. Wang (2002), An improved in situ and satellite SST analysis for climate, *Journal of Climate*, *15*(13), 1609-

1625, doi:10.1175/1520-0442(2002)015<1609:aiisas>2.0.co;2.

Rienecker, M. M., et al. (2011), MERRA: NASA's Modern-Era Retrospective Analysis for Research and Applications, *Journal of Climate*, *24*(14), 3624-3648, doi:10.1175/jcli-d-11-00015.1.

Russell-Smith, J., et al. (2007), Bushfires 'down under': patterns and implications of contemporary Australian landscape burning, *International Journal of Wildland Fire*, *16*(4), 361-377, doi:10.1071/wf07018.

Sheffield, J., G. Goteti, and E. F. Wood (2006), Development of a 50-year high-resolution global dataset of meteorological forcings for land surface modeling, *Journal of Climate*, *19*(13), 3088-3111, doi:10.1175/jcli3790.1.

Smith, A., N. Lott, and R. Vose (2011), The Integrated Surface Database Recent Developments and Partnerships, *Bulletin of the American Meteorological Society*, *92*(6), 704-708, doi:10.1175/2011bams3015.1.

Smith, E. A., et al. (2007), INTERNATIONAL GLOBAL PRECIPITATION MEASUREMENT (GPM) PROGRAM AND MISSION: AN OVERVIEW, *Measuring Precipitation from Space: Eurainsat and the Future*, *28*, 611-+, doi:10.1007/978-1-4020-5835-6_48.

Spessa, A. C., R. D. Field, F. Pappenberger, A. Langner, S. Englhart, U. Weber, T. Stockdale, F. Siegert, J. W. Kaiser, and J. Moore (submitted), Seasonal forecasting of fire over Kalimantan, Indonesia, *Natural Hazards and Earth System Scicences Discussions*, *2*, 5079-5111, doi:doi:10.5194/nhessd-2-5079-2014.

Stocks, B. J., et al. (2002), Large forest fires in Canada, 1959-1997, *Journal of Geophysical Research-Atmospheres*, *108*(D1), 12, doi:10.1029/2001jd000484.

Tanpipat, V., K. Honda, and P. Nuchaiya (2009), MODIS Hotspot Validation over Thailand, *Remote Sensing*, *1*(4), 1043-1054, doi:10.3390/rs1041043.

Taylor, S. W., and M. E. Alexander (2006), Science, technology, and human factors in fire danger rating: the Canadian experience, *International Journal of Wildland Fire*, *15*(1), 121-135, doi:10.1071/wf05021.

van der Werf, G. R., et al. (2008), Climate regulation of fire emissions and deforestation in equatorial Asia, *Proceedings of the National Academy of Sciences of the United States of America*, *105*(51), 20350-20355, doi:10.1073/pnas.0803375105.

van der Werf, G. R., J. T. Randerson, L. Giglio, G. J. Collatz, M. Mu, P. S. Kasibhatla, D. C. Morton, R. S. DeFries, Y. Jin, and T. T. van Leeuwen (2010), Global fire emissions and the contribution of deforestation, savanna, forest, agricultural, and peat fires (1997-2009), *Atmospheric Chemistry and Physics*, *10*(23), 11707-11735, doi:10.5194/acp-10-11707-2010.

Van Wagner, C. E. (1987), Development and structure of the Canadian Forest Fire Weather Index System*Rep.*, 37 pp, Canadian Forest Service, Ottawa, Canada.

Veblen, T. T. (1978), Forest preservation in western highlands of Guatemala, *Geographical Review*, *68*(4), 417-434, doi:10.2307/214215.

Wastl, C., C. Schunk, M. Luepke, G. Cocca, M. Conedera, E. Valese, and A. Menzel (2013), Large-scale weather types, forest fire danger, and wildfire occurrence in the Alps, *Agricultural and Forest Meteorology*, *168*, 15-25, doi:10.1016/j.agrformet.2012.08.011.

Wotton, B. M., and M. D. Flannigan (1993), Length of the fire season in a changing climate, *Forestry Chronicle*, *69*(2), 187-192.

Zumbrunnen, T., H. Bugmann, M. Conedera, and M. Buergi (2009), Linking Forest Fire Regimes and Climate-A Historical Analysis in a Dry Inner Alpine Valley, *Ecosystems*, *12*(1), 73-86, doi:10.1007/s10021-008-9207-3.

Tables

Table 1. Weather stations used for comparison to gridded calculations. Abbreviations are as follows: Environment Canada (EnvCan), GTS (Global Telecommunications System), Canadian Forest Service Northern Forestry Centre (NoFC), National Oceanic and Atmospheric Administration National Climatic Data Center (NCDC), Canadian Forest Service Great Lakes Forestry Centre (GLFC), Australian Bureau of Meteorology (BoM), Thailand Meteorology Department (TMD), Malaysian Meteorological Department (MMD). Environment Canada stations are specified by their agency identifiers and World Meteorological Organization (WMO) identifiers when available. All other stations are are specified by their WMO identifiers. For the NCDC stations, data completeness and periods used in the analysis are provided as part of the data distribution.

ID	Name	Country	Lat.	Lon.	Source	Start year	End year
1123970 (71203)	Kelowna	Canada	49.88	-119.48	EnvCan	1980	2006
1126150 (71889)	Penticton	Canada	49.48	-119.58	EnvCan	1980	1998
5050960 (--)	Flin Flon	Canada	54.77	-101.85	EnvCan	1980	1999
5052880 71867	The Pas	Canada	53.82	-101.25	EnvCan	1980	1999
6072225 (--)	Earlton	Canada	47.71	-79.83	EnvCan	1980	1999
7098600 (71725)	Val-dOr	Canada	48.10	-77.78	EnvCan	1980	1995
760016	Mexicali	Mexico	32.63	-117.00	GTS-NoFC	1999	2012
760023	Tijuana	Mexico	32.55	-116.97	GTS-NoFC	1999	2012
786270	Huehuetenango	Guatemala	15.32	-91.47	GTS-NoFC	1999	2012
786410	Guatemala City	Guatemala	14.58	-90.52	GTS-NoFC	1999	2012
836120	Campo Grande	Brazil	-20.45	-54.72	NCDC	1980	2012
833620	Cuiaba	Brazil	-15.65	-56.10	NCDC	1980	2012
24600	Stockholm Arlanda	Sweden	59.65	17.95	GTS-NoFC	2001	2012
24640	Stockholm Bromma	Sweden	59.35	17.95	GTS-NoFC	2001	2012
29740	Helsinki Vantaa	Finland	61.32	24.97	GTS-NoFC	2004	2012
29750	Helsinki Malmi	Finland	61.25	25.05	GTS-NoFC	2001	2012
106160	Hahn	Germany	49.95	7.27	GTS-NoFC	2001	2012
107080	Saarbruecken	Germany	49.22	7.12	GTS-NoFC	2001	2012
286960	Kalachinsk	Russia	55.03	74.58	NCDC-GLFC	1980	2010
296360	Toguchin	Russia	55.23	84.40	NCDC-GLFC	1980	2010

80010	La Coruna	Spain	43.37	-8.42	NCDC	1980	2012
80420	Santiago	Spain	42.89	-8.41	NCDC	1980	2012
83910	Seville	Spain	37.42	-5.88	NCDC	1980	2012
84100	Cordoba	Spain	37.84	-4.85	NCDC	1980	2012
160880	Brescia	Italy	45.42	10.28	NCDC	1980	2012
160900	Verona	Italy	45.39	10.87	NCDC	1980	2012
166430	Aktion	Greece	38.62	20.77	NCDC	1980	2012
166820	Andravida	Greece	37.91	22.00	NCDC	1980	2012
483270	Chiang Mai	Thailand	18.77	98.97	TMD, NCDC	1980	2012
483030	Chiang Rai	Thailand	19.96	99.88	TMD, NCDC	1980	2012
484050	Roi Et	Thailand	16.12	103.77	TMD, NCDC	1980	2012
484070	Ubon Ratchathani	Thailand	15.25	104.87	TMD, NCDC	1980	2012
486500	Kuala Lumpur IA	Malaysia	3.08	101.65	MMD	2005	2012
486480	Petaling Jaya	Malaysia	3.08	101.65	MMD	2005	2012
964710	Kota Kinabalu	Malaysia	5.93	116.05	MMD	2004	2012
964910	Sandakan	Malaysia	5.25	118.00	MMD	2004	2012
962210	Palembang	Indonesia	-3.00	104.75	NCDC	1980	2012
962370	Pankalpinang	Indonesia	-3.00	104.75	NCDC	1980	2012
966550	Palangkaraya	Indonesia	-1.00	114.00	NCDC	1980	2012
966450	PangkalanBun	Indonesia	-2.70	111.70	NCDC	1980	2012
948650	Laverton	Australia	-37.86	144.76	BoM	1980	2012
948660	Melbourne	Australia	-37.67	144.83	BoM	1980	2012
942380	Tennant Creek	Australia	-19.64	134.18	BoM	1980	2012
943260	Alice Springs	Australia	-23.80	133.89	BoM	1980	2012
946380	Esperance	Australia	-33.83	121.89	BoM	1980	2012
946370	Kalgoorlie-Boulder	Australia	-30.78	121.45	BoM	1980	2012
947670	Sydney	Australia	-33.95	151.00	BoM	1980	2012
947760	Williamtown	Australia	-32.50	151.00	BoM	1980	2012

1

Figures

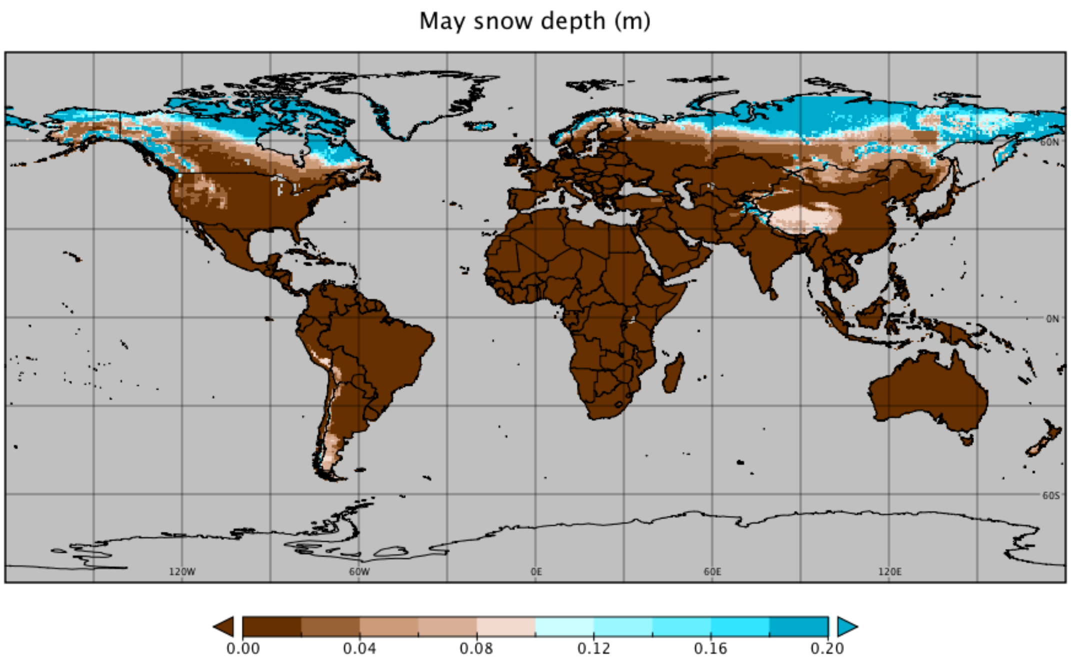

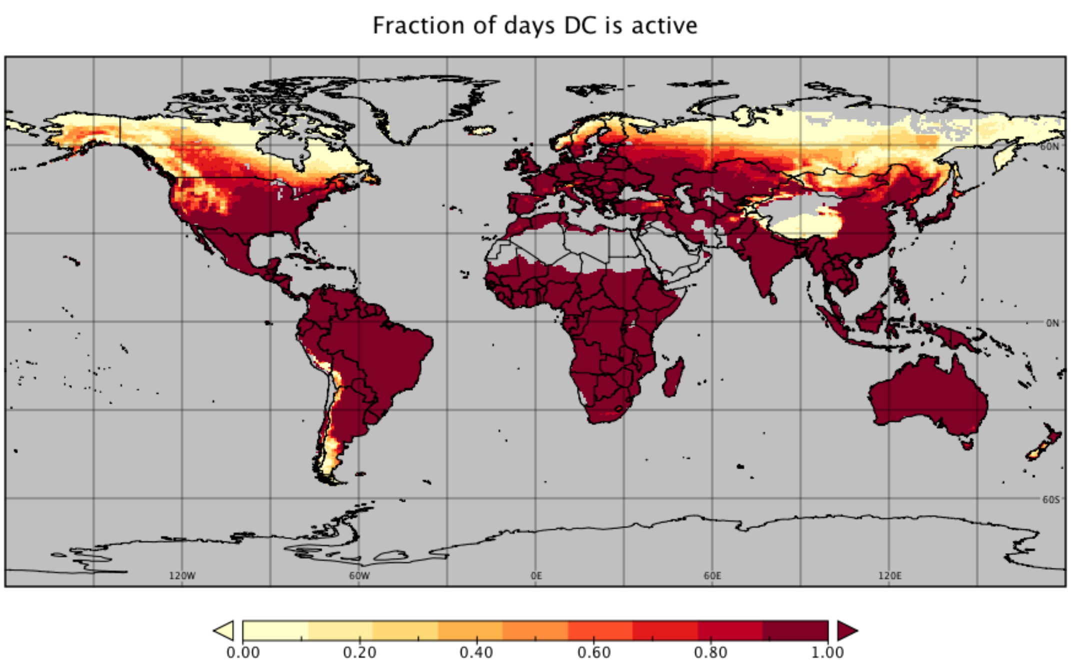

Figure 1. Mean MERRA snow depth (top) and fraction of active DC calculation days (bottom) for May, 1980-2012.

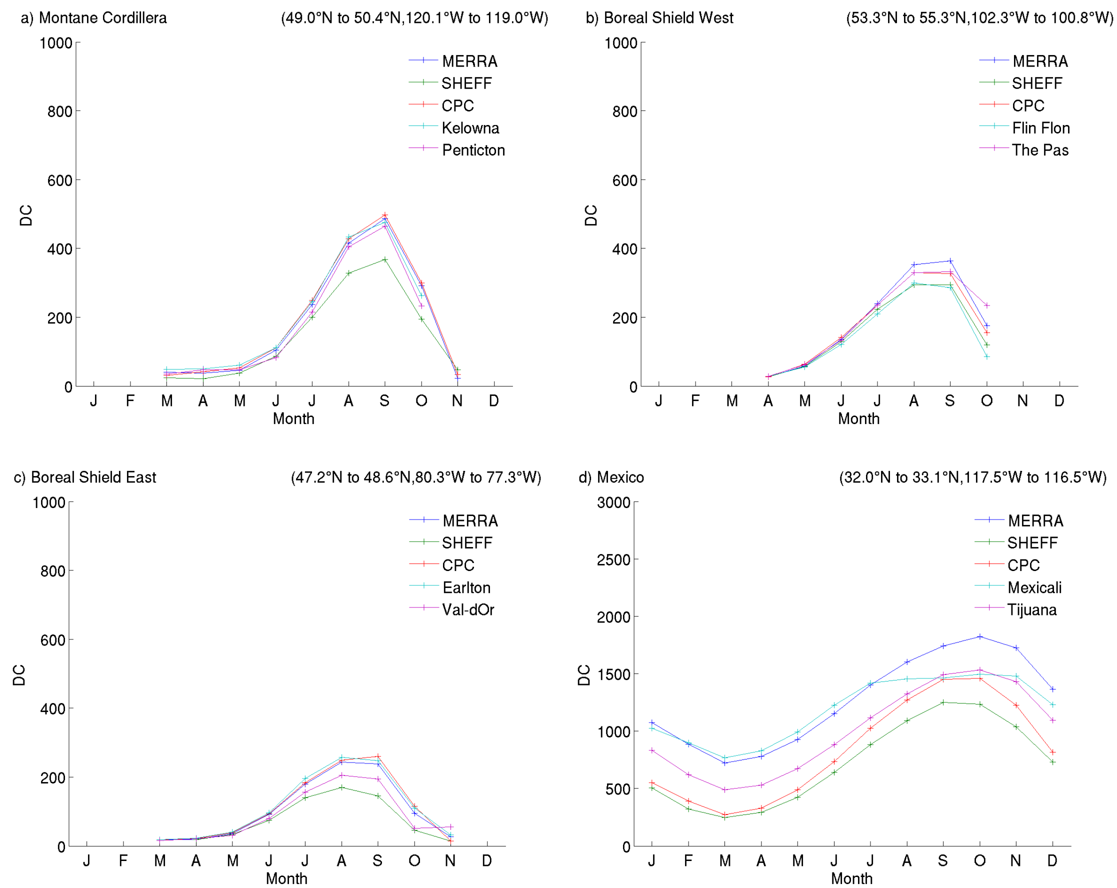

Figure 2. Monthly mean Drought Code (DC) for three regions in Canada and northwestern Mexico. Note the different DC scale for Mexico.

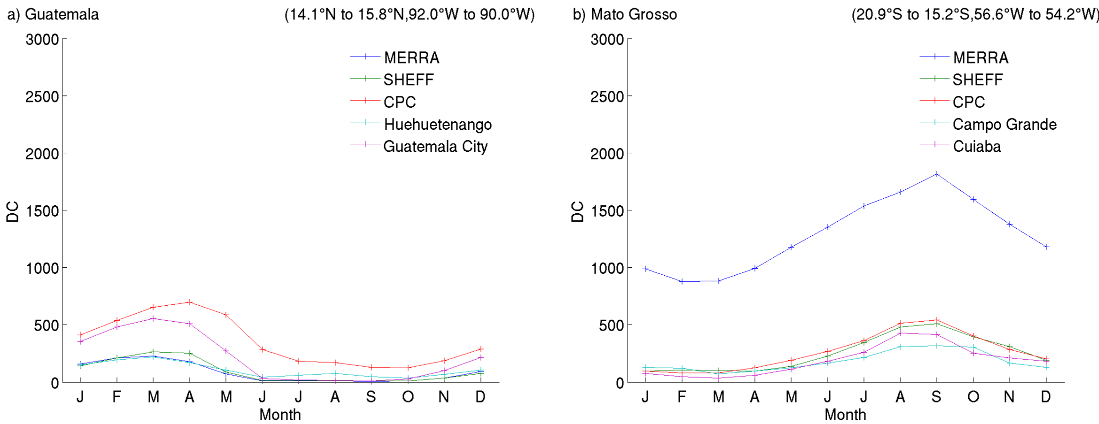

Figure 3. Monthly mean DC for Guatemala and the Mato Grosso of Brazil.

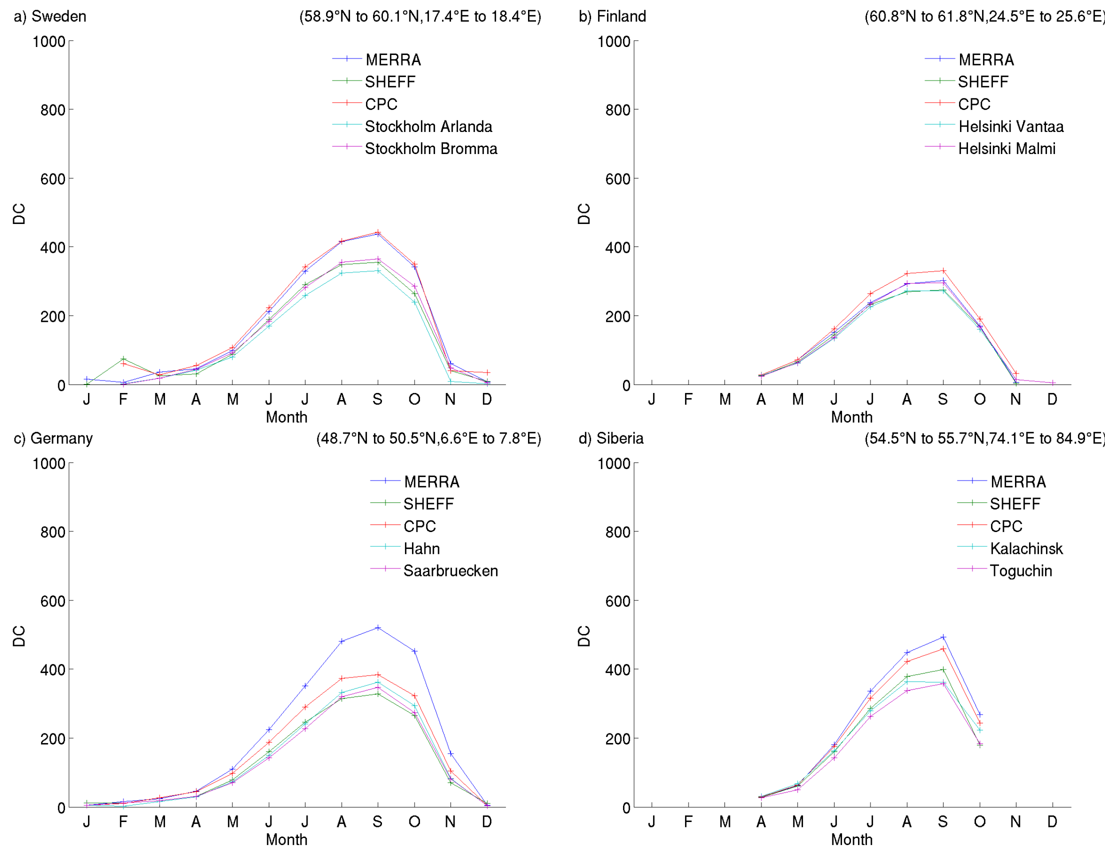

Figure 4. Monthly mean DC for Northern Europe and Siberia

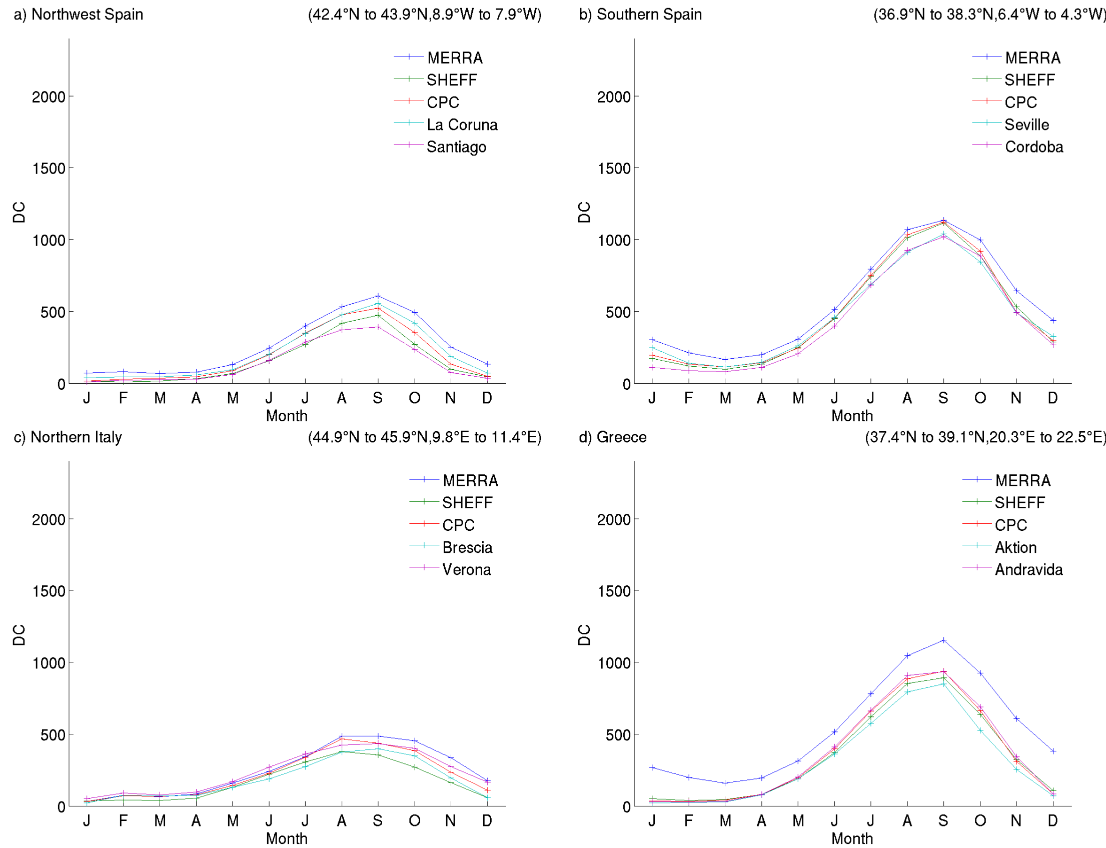

Figure 5. Monthly mean DC for four regions in Southern Europe.

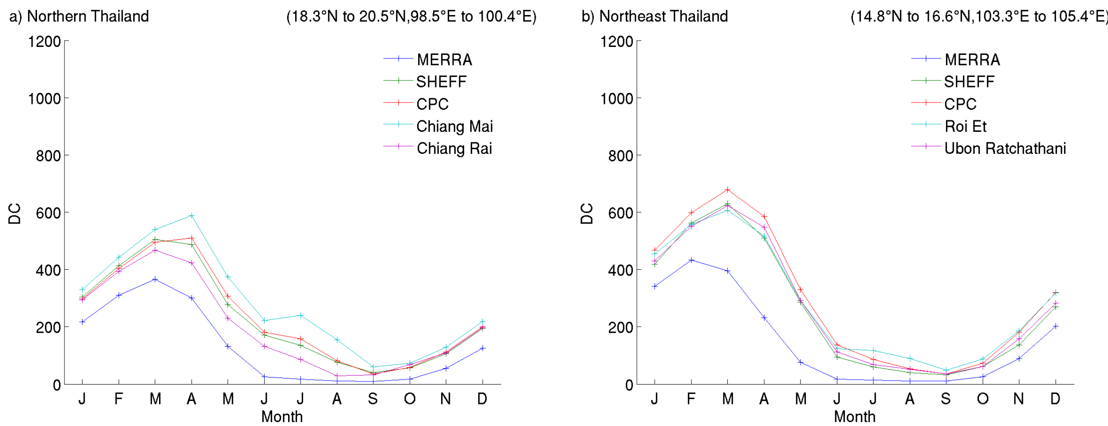

Figure 6. Monthly mean DC for two regions in Thailand.

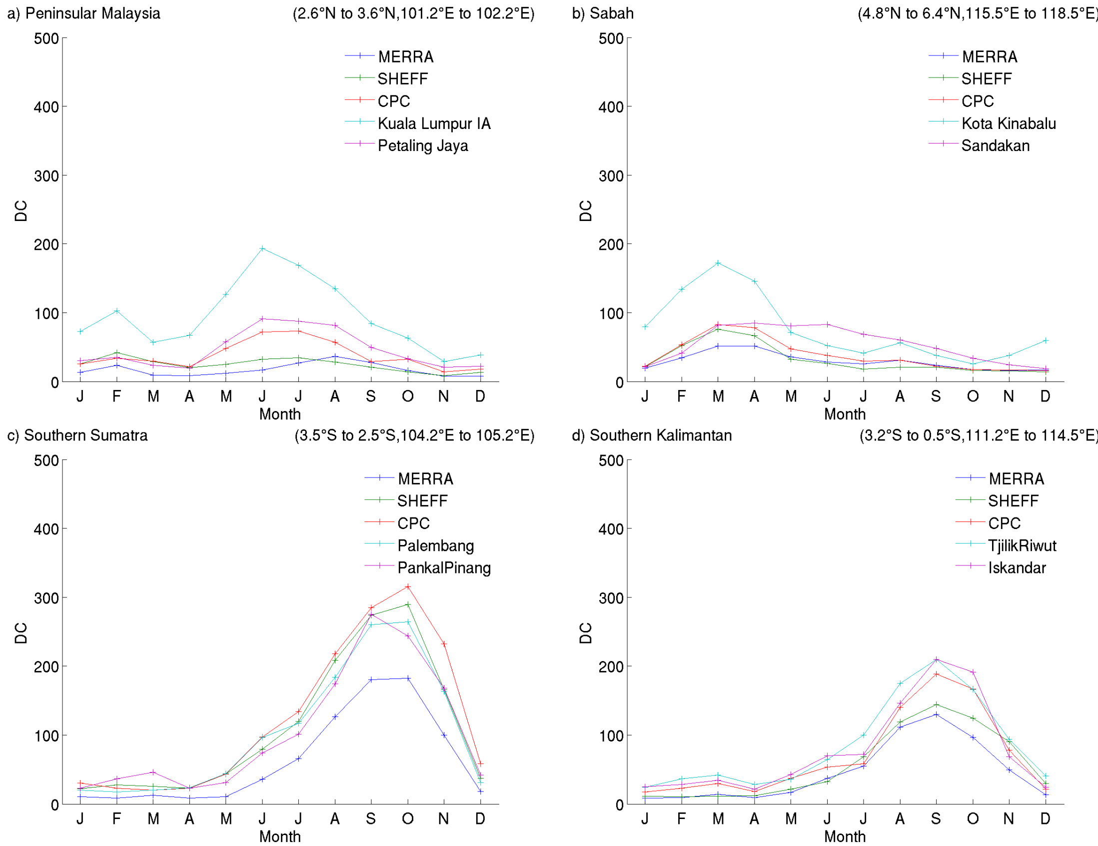

Figure 7. Monthly mean DC for two regions in each of Malaysia and Indonesia.

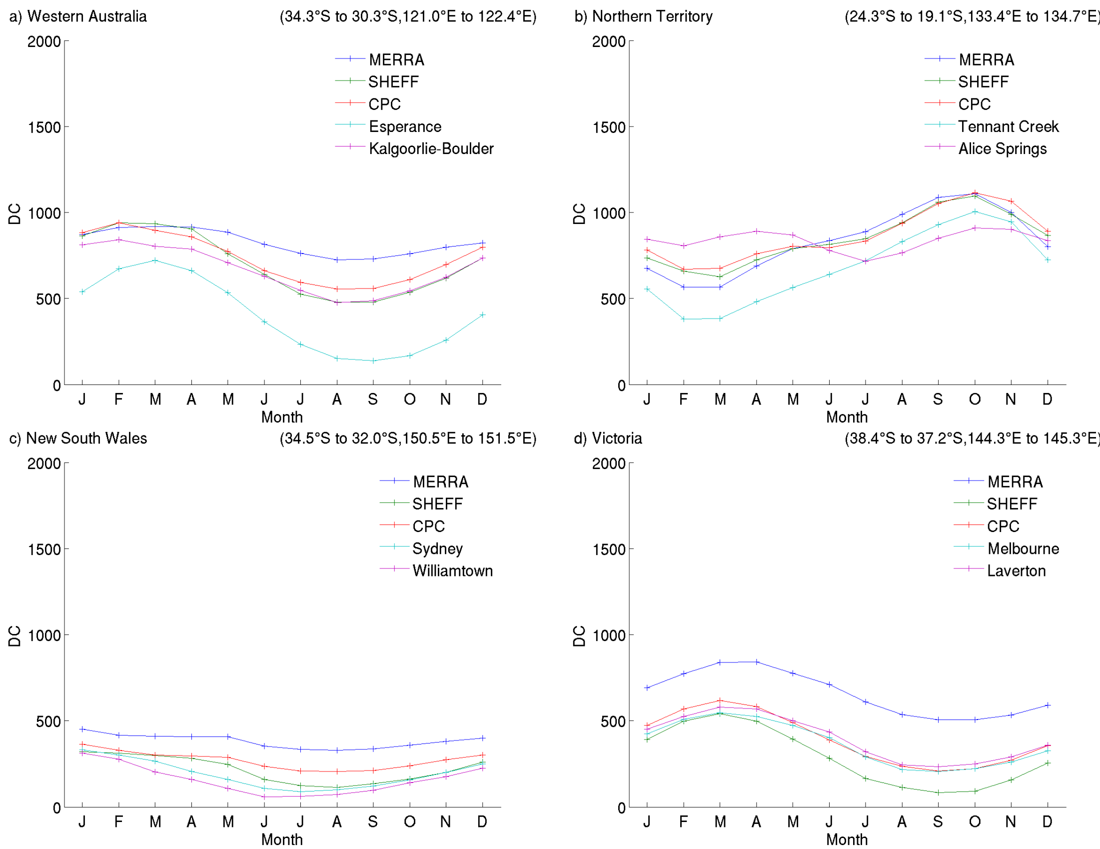

Figure 8. Monthly mean DC for four regions in Australia.

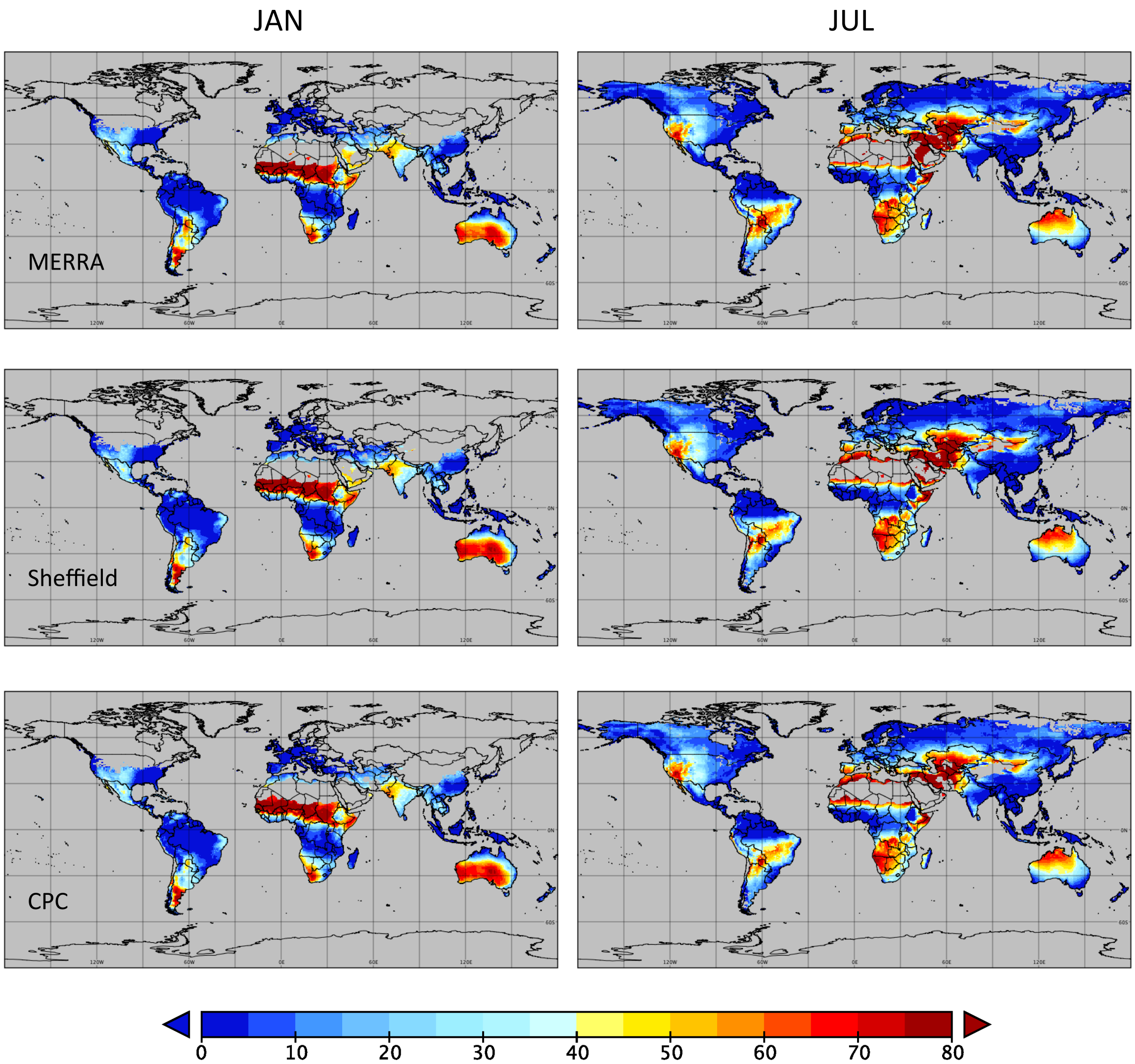

Figure 9. Global gridded mean FWI for January and July based on MERRA precipitation (1980-2012), Sheffield precipitation (1980-2008), and CPC precipitation (1980-2012).

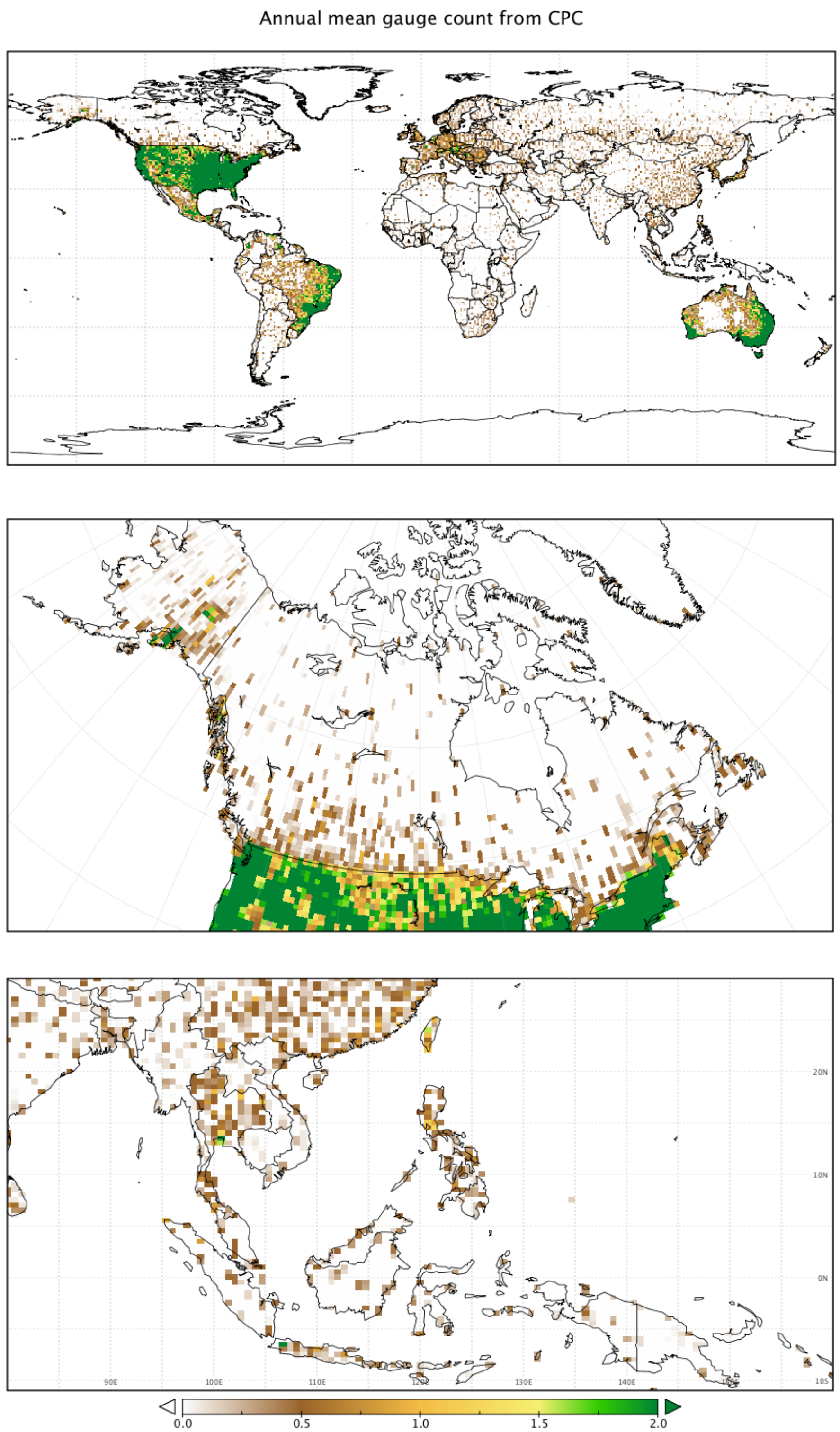

Figure 10. ~~Average~~ Mean 1979-2012 CPC rain gauge coverage (gauges / grid cell) for the globe (top), Canada (middle), Southeast Asia (bottom).